State space modeling of multidien cyclical progression of epilepsy

Krishnakant V. Saboo* KRISHNAKANT.SABOO@UCSF.EDU
University of California San Francisco, USA

Yurui Cao* YURUIC2@ILLINOIS.EDU
University of Illinois Urbana-Champaign, USA

Vaclav Kremen KREMEN.VACLAV@MAYO.EDU
Mayo Clinic, USA; Czech Technical University in Prague, Czech Republic

Suguna Pappu SPAPPU@ILLINOIS.EDU
University of Illinois Urbana-Champaign, USA

Philippa J. Karoly KAROLY.P@UNIMELB.EDU.AU
University of Melbourne, Australia

Dean R. Freestone DEAN@SEERMEDICAL.COM
Seer Medical, Australia

Mark J. Cook MARKCOOK@UNIMELB.EDU.AU
University of Melbourne, Australia

Gregory A. Worrell WORRELL.GREGORY@MAYO.EDU
Mayo Clinic, USA

Ravishankar K. Iyer RKIYER@ILLINOIS.EDU
University of Illinois Urbana-Champaign, USA

Abstract

The risk of seizures in epilepsy fluctuates in cycles with multiday periodicity. The strength of these patient-specific *seizure risk cycles* can be modulated by disease processes. There is a lack of computational models of epilepsy that describe the progression and modulation of multiday seizure risk cycles. We developed a state space model (SSM) for epilepsy progression that learns individualized multiday seizure risk cycles from intracranial EEG (iEEG) data. To capture the cyclical nature of seizure risk, our model incorporated cyclical dynamics by using a special rotation matrix structure for the state transition matrix. The model learned patient-specific multiday cycles using a novel expectation-maximization algorithm. We evaluated the model on real-world data from one of the longest continuous iEEG recordings in people with epilepsy. The model forecast iEEG and inferred periods of heightened risk of seizures better than or comparable to baseline models, and provided novel insight into biological factors that modulate seizure risk cycles. To demonstrate the value of the model in developing brain stimulation treatment, the proposed SSM was integrated with reinforcement learning to reduce seizure risk *in silico*. Our model holds significant potential for addressing clinically important problems.

Keywords: State space model, cyclical dynamics, expectation maximization, epilepsy progression, multiday cycles

Data and Code Availability We used data from the NeuroVista study in which intracranial EEG recordings were obtained in 15 people with epilepsy for up to 2 years each (Cook et al., 2013). De-identified data from the study are publicly available at https://www.epilepsyecosystem.org/. Code: https://github.com/yuruic2/EpilepsySSM

Institutional Review Board (IRB) This research did not require an IRB approval.

1. Introduction

Abnormalities in brain activity are used by clinicians to assess the imminent risk of seizures in people with

* These authors contributed equally.

epilepsy. The risk of seizures fluctuates in cycles with multiday periodicity (Baud et al., 2018). Durations of these *seizure risk cycles* are patient-specific and can be several weeks long. The chance of a seizure occurring can be altered by modulating the strength (amplitude) of these cycles, for e.g., by disease processes (Bower et al., 2017) and medications (Friedrichs-Maeder et al., 2024). There is a lack of computational models of epilepsy that describe the progression and modulation of multiday seizure risk cycles. Such a model can be used to uniquely predict the cycles for each individual, enabling clinically useful applications such as forecasting seizures and developing treatments *in silico*.

We propose a state space model (SSM) of epilepsy progression that learns patient-specific multiday seizure risk cycles and their modulation. We used a state space formulation because it provides a first-order linear system that can be run recursively to generate the complexity of cyclical dynamics in epilepsy. In our SSM, the latent state represents seizure risk. The observations, a patient's brain activity, depend on the latent seizure risk. To capture the cyclical nature of seizure risk, we imposed cyclical dynamics in the latent states by using a special rotation matrix structure for the state transition matrix. This matrix is adopted from Matsuda and Komaki (2017).

There are three main challenges in developing the proposed SSM. (i) *Noisy and limited data*: Brain activity measured by intracranial EEG (iEEG) provides noisy measurements of the seizure risk cycles (Khambhati et al., 2024). Moreover, it is difficult to collect long-term iEEG data from people with epilepsy to estimate weeks-long cycles. (ii) *Weak modulation effects*: Modulations in seizure risk cycles are small and can be difficult to detect in iEEG. This makes it challenging to estimate the effect size of different factors on the cycles. (iii) *Unknown model parameters*: Model parameters are not known *apriori* and need to be learned from limited data.

We addressed these challenges as follows: (i) Long-term iEEG data were used from the NeuroVista study in which iEEG recordings were obtained in 15 people with epilepsy for up to 2 years each (Cook et al., 2013). This is one of the largest datasets of continuous iEEG recordings in epilepsy. The state space formulation enables inferring (latent) seizure risk cycles from noisy iEEG data using a Kalman filter.

(ii) Factors that modulate seizure risk cycles influence the latent state in the model. Since the latent state represents a less noisy estimate of the cycle, it captures small changes in the cycle amplitude. This enables estimating factors that modulate cycles.

(iii) Parameters of the SSM were learned from the iEEG data using a novel Expectation-Maximization (EM) algorithm. Identifiability of parameters is a common issue for learning SSM parameters with EM. Our EM algorithm addresses identifiability by noting that there is a lower limit to the cycle period that can be detected based on the temporal resolution of the model, similar to the Nyquist limit. Imposing this constraint along with the special rotation matrix structure of our model allows EM to learn unique parameters up to a sign. Thus, our approach generalizes the model proposed in Matsuda and Komaki (2017) by relaxing the constraint they imposed on the observation matrix for identifiability.

The value of the proposed model is demonstrated on four applications using synthetic and real-world NeuroVista data. On synthetic data, the proposed EM algorithm recovered the ground truth model parameters, including the duration (period) of multiday cycles. (i) On real data, the proposed model identified ground truth multiday cycles in iEEG features and forecast iEEG values better than or comparable to baseline models. (ii) The latent state of the model can be used to compute the risk of seizures at any given point in time. We found that across patients, seizures occurring within a short interval of each other aligned with periods of heightened seizure risk inferred by the model, highlighting the model's value in forecasting seizures. (iii) The learned model parameters provided novel insight into factors that can influence seizure risk cycles. (iv) Finally, we assessed the usefulness of the model for treatment optimization. We integrated the model with reinforcement learning (RL) to develop a framework for adaptive brain stimulation treatment. In *in silico* experiments, the framework reduced an individual's seizure risk while simultaneously minimizing stimulation.

This paper makes the following contributions:

- We developed an SSM of epilepsy progression that learns personalized multiday seizure risk cycles from iEEG data. To the best of our knowledge, this is among the first models of epilepsy focusing on the timescale of days to months.

- We derived a custom EM algorithm to learn the parameters of the SSM and extended the model proposed in Matsuda and Komaki (2017). Our approach is broadly applicable for model-

ing cyclical dynamics in timeseries, which are observed in several biosignals (Gregg et al., 2023).

- The model forecast iEEG, inferred periods of heightened risk of seizures, and provided novel insight into biological factors that can influence epilepsy progression.
- We demonstrated a framework that combined our SSM with RL and an intuitive reward function for *in silico* optimization of brain stimulation treatment.

1.1. Background

Circadian and multiday cycles have been observed in seizures in people with epilepsy (Baud et al., 2018). Based on these observations, Gregg et al. (2021) proposed a hypothetical descriptive model of seizure risk (Figure 1(a)). The hypothetical model states that seizure risk varies cyclically (or in a combination of cycles). Seizures can occur when the *overall seizure risk* combined across cycles is above a threshold. In addition, seizure generation is probabilistic. Thus, seizures might occur only at some times in the entire duration when the overall seizure risk is above the threshold (Jirsa et al., 2014). A higher amplitude of seizure risk cycles increases the times when seizures are highly likely (Figure 1(a)).

The amplitude of seizure risk cycles can be modified. Anti-seizure medications can decrease the amplitude of multiday seizure risk cycles and reduce seizures (Friedrichs-Maeder et al., 2024). Moreover, seizures influence the risk of future seizures through *consolidation*, i.e., the brain "learns" to seize because of past seizures (Bower et al., 2015, 2017). Since seizure likelihood depends on the cycle amplitude in the hypothetical model, we assumed that consolidation impacts the amplitude of seizure risk cycles.

2. Model

We assumed that there are D unique cycles in the model for a patient (Figure 1(b)). Each cycle is represented by its corresponding angular frequency ω_d, for $d \in \{1, ..., D\}$. The cycle denoted by ω_d has a period of $2\pi/\omega_d$ days. We assumed that there is a hidden seizure risk state $Z_t \in \mathbb{R}^{2D}$ at time t. Each cycle ω_d is represented by two elements $Z_{t,2d-1}, Z_{t,2d} \in \mathbb{R}$ in the latent state Z_t, which capture the seizure risk from cycle ω_d. When the overall seizure risk, i.e., sum of the seizure risk state $\sum_j Z_{t,j}$, is above a certain threshold τ, seizures are very likely. Since consolidation is key to the model and typically occurs during sleep (Stickgold, 2005), the timescale of t is a day.

Based on the hypothetical model proposed by Gregg et al. (2021), we assumed that the latent seizure risk state changes in cycles. In the model, that is achieved through the Markovian relationship:

$$Z_{t+1} = AZ_t, \tag{1}$$

where A is a matrix with complex eigenvalues. We assumed that A has a block diagonal structure, with each block being a rotation matrix corresponding to a unique cycle. Let,

$$\mathcal{R}(\omega_d) = \begin{bmatrix} \cos(\omega_d) & -\sin(\omega_d) \\ \sin(\omega_d) & \cos(\omega_d) \end{bmatrix} \tag{2}$$

be the rotation matrix which rotates the seizure risk state vector by ω_d radians every time. $A = a \times diag(\mathcal{R}(\omega_1), \mathcal{R}(\omega_2), ..., \mathcal{R}(\omega_D))$ where $a \in (0, 1)$ is the norm of the eigenvalues. This structure of A allows the seizure risk from cycle ω_d to evolve independent of the other cycles.

Seizures ($U_t \in \mathbb{R}^M$) can modulate the cycle amplitude through consolidation. Thus, the seizure risk state at the next time point Z_{t+1} depends on the current seizure risk state Z_t and seizures U_t.

$$Z_{t+1} = AZ_t + BU_t + w_t, \tag{3}$$

where $w_t \sim \mathcal{N}(0, \Sigma_w)$ is the system noise. B mediates the consolidation effect of seizures on the seizure risk state. Although seizures U_t are generated from the underlying seizure risk state Z_t, we ignored the edge representing seizure generation for the ease of model training and inference. We did not consider the effect of medications on seizure risk cycles because information about medications is unavailable in the data.

We assumed that the observed iEEG features ($X_t \in \mathbb{R}^M$) depend linearly on the latent seizure risk state Z_t with $v_t \sim \mathcal{N}(0, \Sigma_v)$ measurement noise. The overall SSM is as follows:

$$\begin{gathered} Z_{t+1} = AZ_t + BU_t + w_t \\ X_t = CZ_t + v_t \\ w_t \sim \mathcal{N}(0, \Sigma_w), v_t \sim \mathcal{N}(0, \Sigma_v), Z_0 \sim \mathcal{N}(\mu_0, \Sigma_0) \end{gathered} \tag{4}$$

where the model parameters are $\Theta = \{A, B, C, \Sigma_w, \Sigma_v\, \mu_0, \Sigma_0\}$. We use the following notation to denote the collection of variables over time: $\mathbf{Z} = [Z_0, Z_1, ..., Z_N]$, $\mathbf{X} = [X_0, X_1, ..., X_N]$, and $\mathbf{U} = [U_0, U_1, ..., U_N]$. A vanilla SSM has the same form as Eq. (4) with no constraints on Σ_w and A.

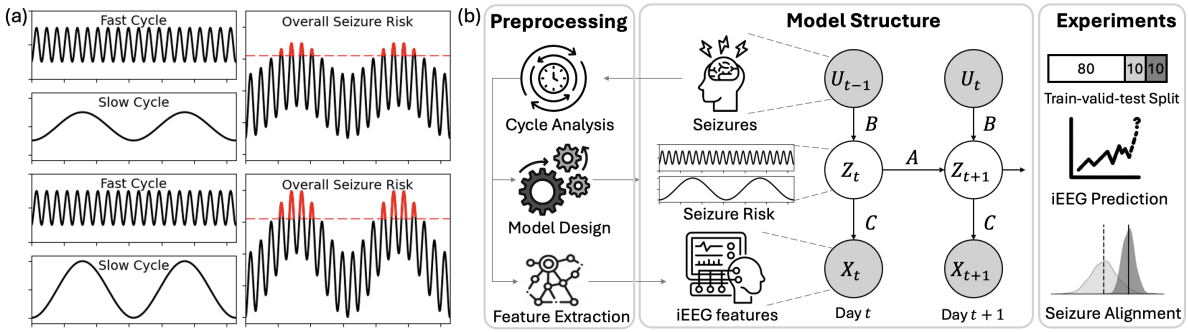

Figure 1: Overview. (a) Hypothetical model of seizure risk (Gregg et al., 2021). A higher amplitude of cycles increases the times when seizures are more likely. (b) Modeling and analysis pipeline. The SSM leverages iEEG data to forecast future iEEG and to infer periods of heightened seizure risk.

3. Expectation-Maximization

We used Expectation-Maximization (EM) to estimate model parameters Θ. Our EM calculations were inspired by Soulat et al. (2022); Wang et al. (2022b) (Appendix A). We assumed that $\Sigma_0 = \sigma_0^2 I$, $\Sigma_w = \sigma_w^2 I$ and $\Sigma_v = \sigma_v^2 I$ where $\sigma_0, \sigma_w, \sigma_v$ are scalars. Without loss of generality, we set $\sigma_w^2 = 0.01$.

The complete log likelihood $\mathcal{L}(\mathbf{Z}, \mathbf{X}|\mathbf{U}; \Theta)$:

$$\mathcal{L}(\mathbf{Z}, \mathbf{X}|\mathbf{U}; \Theta) = \log p(\mathbf{Z}, \mathbf{X}|\mathbf{U}; \Theta)$$

The expectation of the complete log likelihood with respect to the posterior over the latent variables is:

$$G(\Theta) = E_{p(\mathbf{Z}|\mathbf{X},\mathbf{U};\Theta)}[\mathcal{L}(\mathbf{Z}, \mathbf{X}|\mathbf{U}; \Theta)]$$

EM alternates between (i) computing $G(\Theta)$ by inferring latent states $\mathbf{Z}$ (E-step) for the current value of Θ, and (ii) updating the model parameters Θ by maximizing $G(\Theta)$ (M-step). The E- and M-steps are repeated alternatively until convergence.

3.1. E-step

The posterior over the latent states $p(\mathbf{Z}|\mathbf{X}, \mathbf{U}; \Theta)$ is obtained via Kalman smoothing. The posterior distribution is Gaussian with parameters: mean $Z_t^N = E[Z_t|\mathbf{X}]$, and covariance $P_{t_1,t_2}^N = E[Z_{t_1}, Z_{t_2}|\mathbf{X}]$. The expectation of complete log likelihood is:

$$G(\Theta) = -\frac{1}{2}\Big\{G(\mu_0, \Sigma_0) + G(C, \Sigma_v) + G(A, B, \Sigma_w)\Big\}$$

The form of each term is provided in Appendix A.

3.2. M-step

Maximizing $G(\Theta)$ with respect to the parameters Θ results in the following update equations:

$$\mu_0 = Z_0^N$$

$$\sigma_0^2 = \frac{1}{2D} tr\Big((Z_0^N - \mu_0)(Z_0^N - \mu_0)^T + P_0^N\Big)$$

$$C = \left(\sum_{t=0}^{N} X_t (Z_t^N)^T\right)\left(\sum_{t=0}^{N} (Z_t^N (Z_t^N)^T + P_t^N)\right)^{-1}$$

$$\sigma_v^2 = \frac{1}{(N+1)M}\sum_{t=0}^{N} tr\big[(X_t - CZ_t^N)(X_t - CZ_t^N)^T + CP_t^N C^T\big]$$

$$\omega_d = \begin{cases} \tan^{-1}\left(\frac{rt(R_d+\Phi_d)}{tr(R_d-\Phi_d)}\right), \text{if } \frac{rt(R_d+\Phi_d)}{tr(R_d-\Phi_d)} \geq 0 \\ \pi + \tan^{-1}\left(\frac{rt(R_d+\Phi_d)}{tr(R_d-\Phi_d)}\right), \text{otherwise} \end{cases}$$

$$B = \left(\sum_{t=1}^{N} (Z_t^N - AZ_{t-1}^N) U_{t-1}^T\right)\left(\sum_{t=1}^{N} U_{t-1} U_{t-1}^T\right)^{-1}$$

In the update for ω_d, $R = \sum_{t=1}^{N} P_{t,t-1}^N + Z_t^N (Z_{t-1}^N)^T$ and $\Phi = \sum_{t=1}^{N} Z_{t-1}^N (BU_{t-1})^T$ are $2D \times 2D$ matrices. R_d is the d^{th} 2×2 block in matrix R.

$$R_d = \begin{bmatrix} R_{2d-1,2d-1} & R_{2d-1,2d} \\ R_{2d,2d-1} & R_{2d,2d} \end{bmatrix}$$

The functions of a 2×2 matrix V are defined as: $rt(V) = V_{21} - V_{12}$ and $tr(V) = V_{11} + V_{22}$.

3.3. Identifiability

A vanilla SSM solved using EM does not have a unique solution. For an invertible matrix Ψ:

$$\begin{aligned} \Psi Z_{t+1} &= \Psi A \Psi^{-1} \Psi Z_t + \Psi B U_t + \Psi w_t \\ X_t &= C \Psi^{-1} \Psi Z_t + \Psi v_t \\ \Psi w_t \sim \mathcal{N}(0, \Psi \Sigma_w \Psi^T), &\Psi v_t \sim \mathcal{N}(0, \Psi \Sigma_v \Psi^T) \end{aligned} \tag{5}$$

which maps onto a vanilla SSM for parameters Θ': $A' = \Psi A \Psi^{-1}$, $B' = \Psi B$, $C' = C\Psi^{-1}$, $\mu_0' = \Psi \mu_0$, $\Sigma_0' = \Psi \Sigma_0 \Psi^T$, $\Sigma_w' = \Psi \Sigma_w \Psi^T$, and $\Sigma_v' = \Psi \Sigma_v \Psi^T$.

We placed additional constraints on the proposed model for identifiability. (i) We assumed $\Sigma_w = 0.01I$. Thus, $\Psi \Psi^T = I$ i.e., Ψ, must be an orthonormal matrix. (ii) By constraining A to have a block diagonal structure with rotation matrices $\mathcal{R}(\omega_d), d = 1..., D$ on the diagonals, we further restricted Ψ only to be a permutation matrix which can shuffle the blocks. (iii) Both rotation matrices $\mathcal{R}(\omega_d)$ and $\mathcal{R}(-\omega_d)$ can fit the data by appropriately adjusting the sign of the columns of Ψ (Appendix A.3). Note that $-\omega_d$ is equivalent to $2\pi - \omega_d$ and corresponds to a cycle duration between 1 to 2 days, which is faster than the Nyquist limit of 2 days for a model with a temporal resolution of one day. Therefore, we restricted $\omega_d \in [0, \pi]\ \forall d$ since we studied cycles that were slower than two days in the data. (iv) On A, we imposed the constraint that $\omega_1 > \omega_2 > ... > \omega_D$, i.e., the blocks are ordered from the largest angle (fastest cycle) to the smallest angle (slowest cycle).

Using the above constraints, for a solution Θ' for the model, we can recover the permutation matrix Ψ by inspecting the ordering of the blocks in A'. Θ can then be obtained as follows: $A = \Psi^T A' \Psi, B = \Psi^T B', C = C'\Psi, \mu_0 = \Psi^T \mu_0'$. These constraints allow the identification of a unique solution up to a sign for each cycle independent of other cycles.

4. Experimental setup

4.1. Synthetic data

We generated synthetic data using Eq. (4) to assess whether the proposed EM algorithm could recover ground truth (known) parameters (Appendix B).

4.2. Real-world data: NeuroVista study

We used iEEG recordings of nine participants from the NeuroVista study (Table 2). iEEG was sampled at 400 Hz from 12 bipolar-referenced electrodes. Detailed methods are provided in Appendices C, D, E.

Seizures: Seizures were detected from iEEG using a published method (Sladky et al., 2022), resulting in 404.2 ± 322.4 seizures per patient. U_t was obtained by extracting features from seizure iEEG and aggregating them across seizures on day t (Appendix C).

iEEG feature timeseries: iEEG features were obtained for each day by pre-processing the data and extracting univariate and bivariate features in seven non-overlapping frequency bands using a methodology similar to Saboo et al. (2023) (Appendix C). To obtain X_t, we selected six to nine iEEG features for each patient that demonstrated multiday cycles based on the cycle period of seizures (Appendix C).

Ground truth cycle periods: Ground truth cycle period for seizures was determined using r-value analysis (Appendix E) (Gregg et al., 2021). Seizures were divided into *clustered* or *isolated* based on the interval between adjacent seizures. In this dataset, multiday cycles were observed in clustered seizures in 8/9 patients, whereas cycles in isolated seizures were observed only in 2/9 patients. We obtained the ground truth multiday cycle period in iEEG features' timeseries using wavelet analysis (Appendix D). iEEG multiday cycles with period similar to seizure cluster cycles were observed in all the patients.

4.3. Model training and comparison

Data split: Each patient's data was divided chronologically with a 80:10:10 training-validation-test split. We used N^{train}, N^{valid}, and N^{test} to denote the length of training, validation, and testing data, respectively. The feature timeseries were detrended and normalized to have unit variance based on the mean and standard deviation of the training data.

Parameter initialization: During training, A was initialized by uniformly sampling D cycles in the range $2-64$ days, where D is the number of multiday cycles. We set the norm of A's eigenvalues $a = 0.999$ based on preliminary analysis. B and C were initialized with uniform random values. At initialization, $\sigma_0^2, \sigma_v^2 = 1$, $\sigma_w^2 = 0.01$, and $\mu_0 = \mathbf{0}$. μ_0, Σ_0 for the validation data was the filtered latent state $Z_{N^{train}}^{N^{train}}$ and covariance was $P_{N^{train}}^{N^{train}}$. For the test data, μ_0, Σ_0 were the filtered latent state $Z_{N^{train}+N^{valid}}^{N^{train}+N^{valid}}$ and covariance $P_{N^{train}+N^{valid}}^{N^{train}+N^{valid}}$, respectively.

Hyperparameters: For synthetic data, 100 initializations (seeds) of the model were trained for 200 epochs each. For real data, 60 initializations were trained for 300 epochs each. For each seed, the model

corresponding to the minimum validation negative log likelihood was considered. For each patient, the seed that achieved the lowest mean squared error in recovering the angles ω_d of the multiday cycles was chosen for further analysis. The number of multiday cycles $D = 2$ or 3 for each patient (Appendix E).

Baseline models: We compared with three baseline models. (i) ***Vanilla SSM***: An SSM with no constraint on the structure of A and trained with vanilla EM. (ii) ***MK SSM***: The SSM proposed by Matsuda and Komaki (2017), which used the same structure of the A matrix as the proposed model and placed an additional constraint that at least one iEEG feature must include all the multiday cycles. (iii) ***LSTM***: A vanilla long short-term memory model with $2D$ hidden states, matching the dimensionality of Z_t. EM calculations for vanilla SSM are provided in Appendix A and implementation details of the baseline models are provided in Appendix F.

4.4. Reinforcement learning for stimulation

The proposed SSM can be used for *in silico* optimization of brain stimulation by leveraging the same biological mechanism as seizure consolidation, but instead to reduce seizure risk cycles. We combined our SSM with RL to select stimulation $Y_t \; \forall \; t$ that affects latent seizure risk state Z_t. Stimulation Y_t affects Z_t via the input matrix B, which captures the effect of seizure consolidation.

$$Z_{t+1} = AZ_t + BU_t + BY_t + w_t, \tag{6}$$

RL was setup as follows: (1) **State**: The latent seizure risk state $Z_t \in \mathbb{R}^{2D}$. (2) **Action**: Stimulation $Y_t \in \mathbb{R}^M$. (3) **Reward**: The agent was penalized when the overall seizure risk was above 95% of the seizure threshold τ. The agent was encouraged to reduce the magnitude of stimulation Y_t, assuming that the magnitude reflects the total stimulation delivered. Overall, the reward function was given by:

$$r(t) = -\max(0, \sum_j Z_{t,j} - 0.95 * \tau) - ||Y_t||^2 \tag{7}$$

(4) **Environment**: Eq. (6) was implemented in the environment to assess the effect of Y_t on Z_t and to provide the state and reward to the RL agent.

In practice, the latent seizure risk Z_t can be estimated using the observations $X_1, \ldots, X_t$ using a Kalman filter in the environment when observations are available. After stimulation, the latent seizure risk can be estimated using Eq (6). See Appendix F for implementation details of the RL framework.

5. Results

5.1. Model fitting on synthetic data

Proposed EM and vanilla EM both estimated cycle periods accurately (ground truth cycle periods: 10, 25, 45 days; cycle periods estimated by proposed EM: 10.00, 24.96, 45.02 days; by vanilla EM: 10.05, 25.27, 44.50 days). However, due to identifiability issues, A recovered from vanilla EM had a higher mean squared error (MSE) than proposed EM (Figure 3, Appendix B). Consequently, the proposed EM also achieved a lower MSE in estimating matrices B and C. Accurate estimation of A enabled the proposed SSM to identify periods of heightened seizure risk better than vanilla SSM (Figure 5). These results highlight the value of the proposed EM in learning cyclical dynamics.

To further assess the proposed EM, we varied the synthetic data characteristics and estimated parameters of these variants. Proposed EM estimated ground truth parameters accurately for different (i) data duration (N), (ii) missingness, (iii) system noise ($\sigma_w^2 I$), and (iv) eigenvalue norm (a) (Appendix B.3).

5.2. Model fitting on real data

The proposed SSM identified ground truth cycle period better than vanilla SSM and MK SSM (Table 1). Across patients, no initialization (seed) of the vanilla SSM or MK SSM recovered all the ground truth cycles. We observed that A recovered by vanilla EM for several initializations had real eigenvalues > 1 (cycle period $= \infty$), which resulted in model divergence. For four patients, A estimated by the vanilla EM had at least one eigenvalue with norm > 1 in all seeds. In contrast, the constraint on A with $a < 1$ ensured that the proposed model did not diverge. MK SSM's requirement that at least one iEEG feature must contain all the D cycles was not satisfied for most patients. This might explain its poor performance in recovering cycles. We did not compare with LSTM because it does not provide cycle periods explicitly.

The proposed SSM also recovered the cycle periods specific to each iEEG feature. Each iEEG feature only contained a subset of all the cycles modeled in a patient. We studied the coefficients of the learned C to evaluate whether the model recovered the correct subset of cycles for each iEEG feature. In theory, if a cycle ω_j is present in an iEEG feature i, then the coefficients $\sqrt{C_{i,2j-1}^2 + C_{i,2j}^2} > 0$, and if the cycle is absent, then $\sqrt{C_{i,2j-1}^2 + C_{i,2j}^2} = 0$. In the

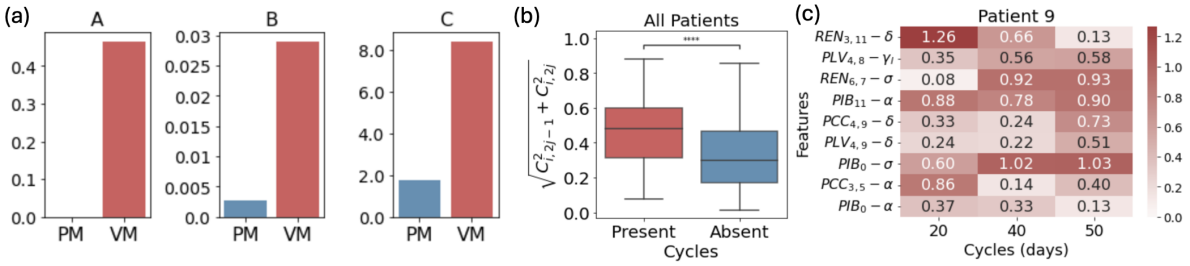

Figure 2: Estimated model parameters for synthetic (a) and real data (b, c). (a) Proposed EM (PM) achieved a lower MSE in estimating model parameters compared to vanilla EM (VM). (b) Coefficients of the observation matrix C were larger for a cycle present in an iEEG feature than for a cycle that was absent, thus, capturing the characteristics of the underlying iEEG data. (c) Coefficients of the input matrix B for Patient 9 were largest for delta (δ) and sigma (σ) bands, which are associated with consolidation. Feature name abbreviation format: $type_{electrode(s)} - band$.

estimated C across patients, we observed that coefficients of C corresponding to a cycle present in iEEG were larger than coefficients of C corresponding to cycles not present in iEEG (Wilcoxon rank-sums test, $p < 10^{-4}$, Figure 2(b)). Thus, the estimated model parameters reflect the underlying data.

5.3. Forecasting iEEG timeseries

Since the SSM captures the generative process of iEEG features X_t, we can forecast iEEG values using the trained model. For each patient, the training and validation data was used to forecast the test data iEEG features. The proposed model achieved comparable or lower forecasting MSE than the baseline models for majority of the patients (Table 1). LSTM achieved slightly lower MSE for 3 patients and substantially better MSE for just one patient compared to the proposed model. We speculate that the competitive performance of the proposed SSM to LSTM could be because of the limited data size. Among SSMs, the proposed model performed better than MK SSM for 7 out of 9 patients and better or comparable to vanilla SSM for 7 patients. This could be because the proposed SSM learned the underlying cyclical dynamics from a small timeseries due to the additional constraints on the proposed EM algorithm.

5.4. Alignment between inferred seizure risk and seizure clusters

Identifying periods of heightened seizure risk is clinically important. We compared the alignment between the occurrence of seizure clusters with the *overall seizure risk* inferred by the model ($\sum_j Z_{t,j}$). We focused on seizure clusters because they lead to worse disease outcomes (Haut, 2015) and since clusters occurred in cycles in this dataset. Overall seizure risk was inferred using the entire iEEG timeseries of a patient because there were few clustered seizures in the test set. We used the filtered latent states to estimate overall seizure risk, i.e., $X_t, \forall t \leq t'$ was used to estimate $Z_{t'}$, which can be valuable to predict the risk of clusters in the next 24 hrs (Khambhati et al., 2024).

For each patient, we computed a metric that we refer to as *Z-distance*, which measures the difference between the distribution of overall seizure risk when seizure clusters occurred with the overall seizure risk when clusters did not occur (Appendix F). A higher *Z-distance* implies that the overall seizure risk is higher at times when seizure clusters occurred compared to times when seizure clusters did not occur. Thus, the overall seizure risk is a meaningful readout of the chance of seizure occurrence, as expected based on the hypothetical model (Figure 1(a)). LSTM was excluded from this analysis because, unlike the SSMs, it does not provide a latent seizure risk state Z_t.

The proposed SSM had a higher *Z-distance* compared to the vanilla SSM and MK SSM for 5/9 patients (Table 1). Two possible reasons for the difference in performance are: (i) In many patients, the vanilla SSM and MK SSM did not recover the multiday cycle whereas the proposed SSM did. (ii) For the vanilla SSM, cycles of different periods may not be represented independently in the latent state Z_t, resulting in errors in the estimation of the phase of each cycle at t (Figure 5, Appendix B). As a result,

Table 1: Results on real data of each patient (ID): Performance of the proposed SSM (PM), vanilla SSM (VM), MK SSM (MK), and LSTM in recovering ground truth (GT) multiday cycles (col: *Multi-day cycle period*), forecasting iEEG (col: *Forecast iEEG*), and inferring heightened seizure risk (col: *Overall sz. risk*). (–) denotes patients for whom the model diverged. Better performance is in bold. *Multi-day cycle period* and *Overall sz. risk* were unavailable for LSTM due to model structure.

ID	Multi-day cycle period (days)				Forecast iEEG (MSE)				Overall sz. risk (*Z-distance*)		
	GT	PM	VM	MK	PM	VM	MK	LSTM	PM	VM	MK
1	(16, 28, 38)	(**15**, 32, **35**)	–	(21, **25**, 707)	**2.6**	–	3.5	5.2	**0.46**	–	0.20
2	(16, 29)	(17, **35**)	–	(**16**, 16)	11.4	–	13.3	**10.8**	**1.33**	–	0.11
3	(22, 32)	(**22**, **31**)	(2, 9)	(5, 24)	34.6	25.9	88.8	**11.1**	0.14	0.04	**0.24**
4	(26, 43, 55)	(**24**, **44**, **47**)	(2, 3, 8)	(43, 46, 47)	1.8	1.6	2.1	**1.3**	0.03	0.05	**0.10**
5	(18, 32, 51)	(**19**, **30**, **43**)	–	(25, 27, 35)	**0.9**	–	1.4	**0.9**	**0.08**	–	0.05
6	(5, 31)	(**5**, **29**)	(3, 16)	(8, 8)	**1.0**	**1.0**	**1.0**	**1.0**	0.25	**0.40**	0.04
7	(18, 28)	(**18**, 32)	(3, **31**)	(2, 20)	**446.2**	**446.2**	**446.2**	471.1	**1.27**	0.25	0.59
8	(7, 22, 50)	(**7**, **21**, **42**)	–	(2, 72, 85)	**9.4**	–	11.7	9.8	0.10	–	**0.24**
9	(20, 40, 50)	(**20**, **45**, **45**)	(2, 2, 10)	(4, 23, 57)	204.6	204.6	1323.2	**202.4**	**0.74**	0.63	0.22

the overall seizure risk will not align with seizures. In the proposed SSM and MK SSM, the block diagonal structure of A ensures that cycles of different periods are independent, which helps with the estimation of overall seizure risk. Since the inferred seizure risk cycles track seizure clusters, the proposed model could potentially forecast seizure clusters.

5.5. Model interpretation: Features related to consolidation modulate cycles

We interpreted the learned input matrix B to identify the iEEG features that modulated seizure risk cycles. In Figure 2(c), a darker square indicates a larger coefficient in B and suggests a larger effect of the corresponding iEEG feature on seizure risk cycles. For Patient 9, the three features that had the largest coefficient in B were delta (0.5 – 4Hz) and sigma (12 – 16Hz) band features. Therefore, seizures with larger feature value in those bands had a larger impact on seizure risk cycles for Patient 9. At least one of the three largest coefficients of B corresponded to a sigma or delta band feature in 7 out of 9 patients (Appendix F). Interestingly, activity in the delta and sigma bands has been linked to sleep-related consolidation (Fogel and Smith, 2011). Thus, our data-driven approach suggested that seizures with larger activity in the bands associated with consolidation have a larger impact on seizure risk cycles. This lends support to the effect of consolidation on seizure risk and can help identify patient-specific factors driving consolidation. Further investigation of consolidation using insights from the model can help identify novel treatments, as shown in Section 5.6.

5.6. RL-based treatment optimization

Since the model captures the effect of consolidation on seizure risk cycles, we investigated whether it can enable *in silico* development of consolidation-based treatment for epilepsy. Stimulation can affect seizure risk through long-term plasticity (Khambhati et al., 2021), which is related to consolidation. We combined the proposed model with RL to drive adaptive brain stimulation applied to Patient 9's model from day 50 onwards (Appendix F). We observed that adaptive stimulation reduced the amplitude of all the seizure cycles but, to a greater extent, the 45-day cycle (Figure 10(b)). Within 105 days of stimulation (day 155), the overall seizure risk was below the seizure threshold τ for most days, implying that the patient receiving this stimulation wouldn't have experienced any further clustered seizures. The magnitude of stimulation also varied over time (Figure 10(c)), demonstrating its adaptive nature.

A limitation of this analysis is that we don't have access to real data from stimulation in Patient 9 to validate the results. We assumed that the input matrix B captures the causal effect of stimulation on epilepsy, which needs to be assessed with real-world

data from stimulation. Moreover, stimulating the brain in a way that generates the Y_t values obtained from this framework may be non-trivial. Nevertheless, this experiment demonstrates how an SSM that learns biologically relevant processes can enable *in silico* development of treatments (Hu et al., 2023).

6. Related work

Modeling epilepsy: Computational models of epilepsy range from biophysically realistic models of neuronal activity (Raikov and Soltesz, 2017, 2019; Liou et al., 2020) to phenomenological models that abstract away the biophysical details and only focus on capturing salient dynamical behaviors of epilepsy (El Houssaini et al., 2020; Kalitzin et al., 2010). Most of these studies model epilepsy-related activity at the short timescale of seconds to minutes. The proposed SSM focuses on a longer timescale of days to months. Rosch et al. (2024) recently proposed a control theoretic approach that models slow (multiday) seizure risk cycles in a single iEEG feature using faster cycles in the same feature. Our approach is demonstrably extensible allowing multiple applications and differs in two main ways. (i) It is unclear how their approach can be extended to handle multiple iEEG features. We observed that, in general, a single iEEG feature did not capture all the multiday seizure cycles. Including multiple features can help forecast seizure risk much better. (ii) The proposed SSM incorporates the effect of other factors (e.g., consolidation) in modulating cycles, whereas their model is driven by the dynamics of a single feature.

Modeling cyclical dynamics: Matsuda and Komaki (2017) developed a SSM to model circular dynamics in the latent states by using rotation matrices as blocks in the state transition matrix. Soulat et al. (2022) and Wodeyar et al. (2021) applied their model to estimate phase-related features of neural signals. For parameter identifiability, their model requires that at least one observed variable must include all the cycles of interest. This requirement is relaxed in the EM algorithm proposed in our work, making our SSM more broadly applicable.

7. Discussion

We developed an SSM of epilepsy progression that learns multiday seizure risk cycles and their modulation from iEEG data and demonstrated its utility for several clinically important problems. Cycles in seizures are widely observed across people with different kinds of epilepsy (Baud et al., 2018; Gregg et al., 2021; Wang et al., 2022a). In principle, our model can be applied to other people with epilepsy beyond the current dataset.The proposed SSM can also be used to model other biosignals that consist of multiday cycles to forecast seizures. Multiday cycles in temperature, heart rate, electrodermal activity, accelerometry data collected from wearables have been linked to seizures (Gregg et al., 2023).

Our approach was applied to chronic data from people with drug-resistant epilepsy. Chronically implanted devices that deliver brain stimulation are proven to reduce seizures, and a viable treatment option for the 30% of epilepsy patients with drug-resistant epilepsy (Ryvlin et al., 2021). The next generation of brain stimulation devices will leverage technological advances to improve outcomes (Denison and Morrell, 2022; Borton et al., 2020). Our approach is suitably positioned to leverage the growing use of these devices and address the need for analytical techniques which handle the complex brain activity data collected from these devices to optimize treatment.

7.1. Limitations

Model: (i) We assumed a linear SSM because of the limited data size. Incorporating non-linear relationships in the observation space could enable the model to capture more variance in the data. (ii) The norm of eigenvalues of A (a) was fixed. Allowing a to be learned during EM will enable the model to better fit the data. Incorporating non-cyclical dynamics in the latent states by adding another block in A will also make the proposed model more flexible. Our EM algorithm can be extended to learn this more flexible model based on the EM approaches provided in Soulat et al. (2022) and Wang et al. (2022b).

Data: (i) We evaluated the model on data from nine patients implanted with an iEEG recording device. Although the dataset is one of the longest continuous iEEG available, validating the model on more patients is important. (ii) Further validation of the RL framework using brain stimulation data is needed (Sladky et al., 2022). (iii) The effect of medications on disease progression was not modelled because that information was unavailable in the dataset. For clinical utility, it is important to include medication data and jointly model the effect of consolidation, medications, and brain stimulation (when delivered).

Acknowledgments

This work was supported by the Mayo Clinic and Illinois Alliance Fellowship for Technology-based Healthcare Research and Schmidt Science Fellows, in partnership with the Rhodes Trust. It was also supported in part by NSF grant CNS-1624790 (CCBGM), European Union's HORIZON EUROPE grant agreement no. 101136607 (CLARA), a grant from Carle Foundation Hospital, and a grant from the Jump ARCHES endowment fund. We thank R. Srikant, Sanmi Koyejo, Vladimir Sladky, and Chang Hu for their valuable feedback and contribution.

References

Maxime O Baud, Jonathan K Kleen, Emily A Mirro, Jason C Andrechak, David King-Stephens, Edward F Chang, and Vikram R Rao. Multi-day rhythms modulate seizure risk in epilepsy. *Nature communications*, 9(1):88, 2018.

David A Borton, Heather E Dawes, Gregory A Worrell, Philip A Starr, and Timothy J Denison. Developing collaborative platforms to advance neurotechnology and its translation. *Neuron*, 108(2): 286–301, 2020.

Mark R Bower, Matt Stead, Regina S Bower, Michal T Kucewicz, Vlastimil Sulc, Jan Cimbalnik, Benjamin H Brinkmann, Vincent M Vasoli, Erik K St Louis, Fredric B Meyer, et al. Evidence for consolidation of neuronal assemblies after seizures in humans. *Journal of Neuroscience*, 35(3):999–1010, 2015.

Mark R Bower, Michal T Kucewicz, Erik K St. Louis, Fredric B Meyer, W Richard Marsh, Matt Stead, and Gregory A Worrell. Reactivation of seizure-related changes to interictal spike shape and synchrony during postseizure sleep in patients. *Epilepsia*, 58(1):94–104, 2017.

Greg Brockman, Vicki Cheung, Ludwig Pettersson, Jonas Schneider, John Schulman, Jie Tang, and Wojciech Zaremba. Openai gym, 2016.

Mark J Cook, Terence J O'Brien, Samuel F Berkovic, Michael Murphy, Andrew Morokoff, Gavin Fabinyi, Wendyl D'Souza, Raju Yerra, John Archer, Lucas Litewka, et al. Prediction of seizure likelihood with a long-term, implanted seizure advisory system in patients with drug-resistant epilepsy: a first-in-man study. *The Lancet Neurology*, 12(6):563–571, 2013.

Tim Denison and Martha J Morrell. Neuromodulation in 2035: the neurology future forecasting series. *Neurology*, 98(2):65–72, 2022.

Kenza El Houssaini, Christophe Bernard, and Viktor K Jirsa. The epileptor model: a systematic mathematical analysis linked to the dynamics of seizures, refractory status epilepticus, and depolarization block. *Eneuro*, 7(2), 2020.

Stuart M Fogel and Carlyle T Smith. The function of the sleep spindle: a physiological index of intelligence and a mechanism for sleep-dependent memory consolidation. *Neuroscience & Biobehavioral Reviews*, 35(5):1154–1165, 2011.

Cecilia Friedrichs-Maeder, Timothée Proix, Thomas K Tcheng, Tara Skarpaas, Vikram R Rao, and Maxime O Baud. Seizure cycles under pharmacotherapy. *Annals of neurology*, 95(4): 743–753, 2024.

Nicholas M Gregg, Vladimir Sladky, Petr Nejedly, Filip Mivalt, Inyong Kim, Irena Balzekas, Beverly K Sturges, Chelsea Crowe, Edward E Patterson, Jamie J Van Gompel, et al. Thalamic deep brain stimulation modulates cycles of seizure risk in epilepsy. *Scientific reports*, 11(1):24250, 2021.

Nicholas M Gregg, Tal Pal Attia, Mona Nasseri, Boney Joseph, Philippa Karoly, Jie Cui, Rachel E Stirling, Pedro F Viana, Thomas J Richner, Ewan S Nurse, et al. Seizure occurrence is linked to multiday cycles in diverse physiological signals. *Epilepsia*, 64(6):1627–1639, 2023.

Sheryl R Haut. Seizure clusters: characteristics and treatment. *Current opinion in neurology*, 28(2): 143–150, 2015.

Chang Hu, Krishnakant V Saboo, Ahmad H Ali, Brian D Juran, Konstantinos N Lazaridis, and Ravishankar K Iyer. Remedi: Reinforcement learning-driven adaptive metabolism modeling of primary sclerosing cholangitis disease progression. In *Machine Learning for Health (ML4H)*, pages 157–189. PMLR, 2023.

Viktor K Jirsa, William C Stacey, Pascale P Quilichini, Anton I Ivanov, and Christophe Bernard.

On the nature of seizure dynamics. *Brain*, 137(8): 2210–2230, 2014.

Stiliyan N Kalitzin, Demetrios N Velis, and Fernando H Lopes da Silva. Stimulation-based anticipation and control of state transitions in the epileptic brain. *Epilepsy & Behavior*, 17(3):310–323, 2010.

Philippa J Karoly, Daniel M Goldenholz, Dean R Freestone, Robert E Moss, David B Grayden, William H Theodore, and Mark J Cook. Circadian and circaseptan rhythms in human epilepsy: a retrospective cohort study. *The Lancet Neurology*, 17 (11):977–985, 2018.

Ankit N Khambhati, Alia Shafi, Vikram R Rao, and Edward F Chang. Long-term brain network reorganization predicts responsive neurostimulation outcomes for focal epilepsy. *Science Translational Medicine*, 13(608):eabf6588, 2021.

Ankit N Khambhati, Edward F Chang, Maxime O Baud, and Vikram R Rao. Hippocampal network activity forecasts epileptic seizures. *Nature medicine*, pages 1–4, 2024.

Jyun-you Liou, Elliot H Smith, Lisa M Bateman, Samuel L Bruce, Guy M McKhann, Robert R Goodman, Ronald G Emerson, Catherine A Schevon, and LF Abbott. A model for focal seizure onset, propagation, evolution, and progression. *Elife*, 9:e50927, 2020.

Takeru Matsuda and Fumiyasu Komaki. Multivariate time series decomposition into oscillation components. *Neural Computation*, 29(8):2055–2075, 2017.

Ivan Raikov and Ivan Soltesz. Hippocampal in silico models of seizures and epilepsy. In *Models of Seizures and Epilepsy*, pages 219–232. Elsevier, 2017.

Ivan Raikov and Ivan Soltesz. Data-driven modeling of normal and pathological oscillations in the hippocampus. *Multiscale Models of Brain Disorders*, pages 185–192, 2019.

Richard E Rosch, Brittany Scheid, Kathryn A Davis, Brian Litt, and Arian Ashourvan. Epileptiform activity and seizure risk follow long-term non-linear attractor dynamics. *bioRxiv*, pages 2024–07, 2024.

Philippe Ryvlin, Sylvain Rheims, Lawrence J Hirsch, Arseny Sokolov, and Lara Jehi. Neuromodulation in epilepsy: state-of-the-art approved therapies. *The Lancet Neurology*, 20(12):1038–1047, 2021.

Krishnakant V Saboo, Yurui Cao, Vaclav Kremen, Vladimir Sladky, Nicholas M Gregg, Paul M Arnold, Philippa J Karoly, Dean R Freestone, Mark J Cook, Gregory A Worrell, et al. Individualized seizure cluster prediction using machine learning and ambulatory intracranial eeg. In *2022 IEEE International Conference on Bioinformatics and Biomedicine (BIBM)*, pages 1157–1163. IEEE, 2022.

Krishnakant V Saboo, Yurui Cao, Vaclav Kremen, Vladimir Sladky, Nicholas M Gregg, Paul M Arnold, Philippa J Karoly, Dean R Freestone, Mark J Cook, Gregory A Worrell, et al. Individualized seizure cluster prediction using machine learning and chronic ambulatory intracranial eeg. *IEEE Transactions on NanoBioscience*, 2023.

John Schulman, Sergey Levine, Pieter Abbeel, Michael Jordan, and Philipp Moritz. Trust region policy optimization. In *International conference on machine learning*, pages 1889–1897. PMLR, 2015.

Vladimir Sladky, Petr Nejedly, Filip Mivalt, Benjamin H Brinkmann, Inyong Kim, Erik K St. Louis, Nicholas M Gregg, Brian N Lundstrom, Chelsea M Crowe, Tal Pal Attia, et al. Distributed brain co-processor for tracking spikes, seizures and behaviour during electrical brain stimulation. *Brain Communications*, 4(3):fcac115, 2022.

Hugo Soulat, Emily P Stephen, Amanda M Beck, and Patrick L Purdon. State space methods for phase amplitude coupling analysis. *Scientific Reports*, 12 (1):15940, 2022.

Robert Stickgold. Sleep-dependent memory consolidation. *Nature*, 437(7063):1272–1278, 2005.

Christopher Torrence and Gilbert P Compo. A practical guide to wavelet analysis. *Bulletin of the American Meteorological society*, 79(1):61–78, 1998.

Emily T Wang, Marina Vannucci, Zulfi Haneef, Robert Moss, Vikram R Rao, and Sharon Chiang. A bayesian switching linear dynamical system for estimating seizure chronotypes. *Proceedings of the National Academy of Sciences*, 119(46): e2200822119, 2022a.

Qinxia Wang, Ji Meng Loh, Xiaofu He, and Yuanjia Wang. A latent state space model for estimating brain dynamics from electroencephalogram (eeg) data. *Biometrics*, 2022b.

Anirudh Wodeyar, Mark Schatza, Alik S Widge, Uri T Eden, and Mark A Kramer. A state space modeling approach to real-time phase estimation. *Elife*, 10:e68803, 2021.

Appendix A. EM calculations

The complete likelihood $p(\mathbf{Z}, \mathbf{X}|\mathbf{U})$ of the model is:

$$
\begin{aligned}
&p(\mathbf{Z}, \mathbf{X}|\mathbf{U}; \Theta) \\
&= p(Z_0, Z_1, ..., Z_N, X_0, X_1, ..., X_N|U_0, U_1, ..., U_N; \Theta) \\
&= p(X_0|Z_0, \{U_{t'}\}_{t'=0}^{N}; \Theta) p(Z_0|\{U_{t'}\}_{t'=0}^{N}; \Theta) \\
&\quad \prod_{t=1}^{N} \Bigg[p(X_t|Z_t, \{Z_{t'}\}_{t'=0}^{t-1}, \{X_{t'}\}_{t'=0}^{t-1}, \{U_{t'}\}_{t'=0}^{N}; \Theta) \\
&\quad p(Z_t|Z_{t-1}, \{Z_{t'}\}_{t'=0}^{t-2}, \{X_{t'}\}_{t'=0}^{t-1}, \{U_{t'}\}_{t'=0}^{N}; \Theta) \Bigg] \\
&= p(Z_0; \Theta) p(X_0|Z_0; \Theta) \\
&\quad \prod_{t=1}^{N} p(X_t|Z_t; \Theta) p(Z_t|Z_{t-1}, U_{t-1}; \Theta)
\end{aligned} \tag{8}
$$

The complete log likelihood $\mathcal{L}(\mathbf{Z}, \mathbf{X}|\mathbf{U}; \Theta)$ is:

$$
\begin{aligned}
&\mathcal{L}(\mathbf{Z}, \mathbf{X}|\mathbf{U}; \Theta) \\
&= \log p(Z_0; \Theta) + \sum_{t=0}^{N} \log p(X_t|Z_t; \Theta) \\
&\quad + \sum_{t=1}^{N} \log p(Z_t|Z_{t-1}, U_{t-1}; \Theta) \\
&= -\frac{1}{2} \log 2\pi|\Sigma_0| - \frac{1}{2}(Z_0 - \mu_0)^T \Sigma_0^{-1} (Z_0 - \mu_0) \\
&\quad + \sum_{t=0}^{N} \Bigg[-\frac{1}{2} \log 2\pi|\Sigma_v| \\
&\quad -\frac{1}{2}(X_t - CZ_t)^T \Sigma_v^{-1} (X_t - CZ_t) \Bigg] \\
&\quad + \sum_{t=1}^{N} \Bigg[-\frac{1}{2} \log 2\pi|\Sigma_w| \\
&\quad - \frac{1}{2}(Z_t - AZ_{t-1} - BU_{t-1})^T \Sigma_w^{-1} \\
&\quad \times (Z_t - AZ_{t-1} - BU_{t-1}) \Bigg] \\
&= -\frac{1}{2} \Bigg\{ \log|\Sigma_0| + (Z_0 - \mu_0)^T \Sigma_0^{-1} (Z_0 - \mu_0) \\
&\quad + (N+1) \log|\Sigma_v| \\
&\quad + \sum_{t=0}^{N} (X_t - CZ_t)^T \Sigma_v^{-1} (X_t - CZ_t) \\
&\quad + N \log|\Sigma_w|
\end{aligned}
$$

$$+\sum_{t=1}^{N}\Bigg[(Z_t - AZ_{t-1} - BU_{t-1})^T\Sigma_w^{-1} \times (Z_t - AZ_{t-1} - BU_{t-1})\Bigg]\Bigg\} \quad (9)$$

A.1. E-step

The Kalman smoother equations are as follow. Let $Z_t^{t-1} = E[Z_t|\{X_{t'}\}_{t'=1}^{t-1}]$ and $P_t^{t-1} = Cov[Z_t|\{X_{t'}\}_{t'=1}^{t-1}]$. The forward pass is given as follows:

$$\begin{aligned} Z_t^{t-1} &= AZ_{t-1}^{t-1} + BU_{t-1} \\ P_t^{t-1} &= AP_{t-1}^{t-1}A^T + \Sigma_w \\ K_t &= P_t^{t-1}C^T(CP_t^{t-1}C^T + \Sigma_v)^{-1} \\ Z_t^t &= Z_t^{t-1} + K_t(X_t - CZ_t^{t-1}) \\ P_t^t &= P_t^{t-1} - K_tCP_t^{t-1} \end{aligned}$$

Let $Z_t^N = E[Z_t|\mathbf{X}]$ and $P_{t_1,t_2}^N = E[Z_{t_1}, Z_{t_2}|\mathbf{X}]$. Thus, the Backward pass can be given as:

$$\begin{aligned} J_{t-1} &= P_{t-1}^{t-1}A^T(P_t^{t-1})^{-1} \\ Z_{t-1}^N &= Z_{t-1}^{t-1} + J_{t-1}(Z_t^N - Z_t^{t-1}) \\ P_{t-1}^N &= P_{t-1}^{t-1} + J_{t-1}(P_t^N - P_t^{t-1})J_{t-1}^T \\ P_{t_1,t_2}^N &= J_{t_1}P_{t_1+1,t_2}^N \end{aligned}$$

Using the above Kalman smoother equations for computing the E-step, we get:

$$\begin{aligned} G(\Theta) &= E_{p(\mathbf{Z}|\mathbf{X},\mathbf{U};\Theta)}[\mathcal{L}(\mathbf{Z},\mathbf{X}|\mathbf{U};\Theta)] \\ &= -\frac{1}{2}\Bigg\{G(\mu_0,\Sigma_0) + G(C,\Sigma_v) + G(A,B,\Sigma_w)\Bigg\} \end{aligned} \quad (10)$$

Recall that $\Sigma_0 = \sigma_0^2 I_{2D\times 2D}$ where D is the number of cycles in the model. Let,

$$\begin{aligned} &G(\mu_0,\Sigma_0) \\ &= \log|\Sigma_0| + tr\left(\Sigma_0^{-1}((Z_0^N - \mu_0)(Z_0^N - \mu_0)^T + P_0^N)\right) \\ &= \log(\sigma_0^2)^{2D} + \frac{1}{\sigma_0^2}tr\left((Z_0^N - \mu_0)(Z_0^N - \mu_0)^T) + P_0^N\right) \\ &= 2D\log\sigma_0^2 + \frac{1}{\sigma_0^2}tr\left((Z_0^N - \mu_0)(Z_0^N - \mu_0)^T + P_0^N\right) \end{aligned} \quad (11)$$

Recall that $\Sigma_v = \sigma_v^2 I_{M\times M}$ where $X_t \in \mathbb{R}^M$ is the dimensionality of the observed data. Let,

$$\begin{aligned} &G(C,\Sigma_v) = (N+1)\log|\Sigma_v| \\ &+\sum_{t=0}^{N} tr\Bigg(\Sigma_v^{-1}((X_t - CZ_t^N)(X_t - CZ_t^N)^T \\ &+ CP_t^NC^T)\Bigg) \\ &= (N+1)M\log\sigma_v^2 \\ &+ \frac{1}{\sigma_v^2}\sum_{t=0}^{N} tr\Bigg((X_t - CZ_t^N)(X_t - CZ_t^N)^T \\ &+ CP_t^NC^T\Bigg) \end{aligned} \quad (12)$$

$$\begin{aligned} &G(A,B,\Sigma_w) \\ &= N\log|\Sigma_w| \\ &+ E_{p(Z|X,U;\Theta)}\Bigg[\sum_{t=1}^{N}(Z_t - AZ_{t-1} - BU_{t-1})^T\Sigma_w^{-1} \\ &\times (Z_t - AZ_{t-1} - BU_{t-1})\Bigg] \\ &= N\log|\Sigma_w| \\ &+ E_{p(Z|X,U;\Theta)}\Bigg[\sum_{t=1}^{N}(Z_t - AZ_{t-1})^T\Sigma_w^{-1}(Z_t - AZ_{t-1}) \\ &- (Z_t - AZ_{t-1})^T\Sigma_w^{-1}BU_{t-1} \\ &-(BU_{t-1})^T\Sigma_w^{-1}(Z_t - AZ_{t-1}) \\ &+ (BU_{t-1})^T\Sigma_w^{-1}BU_{t-1}\Bigg] \\ &= N\log|\Sigma_w| \\ &+ E_{p(Z|X,U;\Theta)}\Bigg[\sum_{t=1}^{N}(Z_t - AZ_{t-1})^T\Sigma_w^{-1}(Z_t - AZ_{t-1}) \\ &- 2(BU_{t-1})^T\Sigma_w^{-1}(Z_t - AZ_{t-1}) \\ &+ (BU_{t-1})^T\Sigma_w^{-1}BU_{t-1}\Bigg] \\ &= N\log|\Sigma_w| \\ &+ E_{p(Z|X,U;\Theta)}\Bigg[\sum_{t=1}^{N}(Z_t - AZ_{t-1})^T\Sigma_w^{-1}(Z_t - AZ_{t-1})\Bigg] \end{aligned}$$

$$
\begin{aligned}
&- 2E_{p(Z|X,U;\Theta)}\left[\sum_{t=1}^{N}(BU_{t-1})^T\Sigma_w^{-1}(Z_t - AZ_{t-1})\right] \\
&+ E_{p(Z|X,U;\Theta)}\left[\sum_{t=1}^{N}(BU_{t-1})^T\Sigma_w^{-1}BU_{t-1}\right] \\
&= N\log|\Sigma_w| + tr\left(\Sigma_w^{-1}(S - RA^T - AR^T + AQA^T)\right) \\
&- 2\sum_{t=1}^{N}(BU_{t-1})^T\Sigma_w^{-1}(Z_t^N - AZ_{t-1}^N) \\
&+ \sum_{t=1}^{N}(BU_{t-1})^T\Sigma_w^{-1}BU_{t-1} \qquad (13)
\end{aligned}
$$

where,

$$
\begin{aligned}
Q &= \sum_{t=1}^{N} P_{t-1}^N + Z_{t-1}^N(Z_{t-1}^N)^T \\
R &= \sum_{t=1}^{N} P_{t,t-1}^N + Z_t^N(Z_{t-1}^N)^T \\
S &= \sum_{t=1}^{N} P_t^N + Z_t^N(Z_t^N)^T
\end{aligned}
$$

Substitute $\Sigma_w = \sigma_w^2 I_{2D\times 2D}$ in the Eq. (13) to get:

$$
\begin{aligned}
&G(A,B,\Sigma_w) \\
&= 2ND\log\sigma_w^2 + \frac{1}{\sigma_w^2}tr\left((S - RA^T - AR^T + AQA^T)\right) \\
&- \frac{2}{\sigma_w^2}\sum_{t=1}^{N}U_{t-1}^TB^T(Z_t^N - AZ_{t-1}^N) \\
&+ \frac{1}{\sigma_w^2}\sum_{t=1}^{N}U_{t-1}^TB^TBU_{t-1} \qquad (14)
\end{aligned}
$$

We can further simplify Eq. (14) based on the block diagonal form of $A = a \times diag(\mathcal{R}(\omega_1), \mathcal{R}(\omega_2), ..., \mathcal{R}(\omega_D))$.

Due to A's block diagonal nature, we can simplify matrix multiplication with A. For e.g.,

$$
\begin{aligned}
tr(AR) &= \sum_{d=1}^{D} tr((AR)_d) = \sum_{d=1}^{D} tr(A_dR_d) \\
&= \sum_{d=1}^{D} tr(a\mathcal{R}(\omega_d)R_d)
\end{aligned}
$$

where, R_d is the d^{th} block in matrix R.

$$
R_d = \begin{bmatrix} R_{2d-1,2d-1} & R_{2d-1,2d} \\ R_{2d,2d-1} & R_{2d,2d} \end{bmatrix}
$$

Similarly, for a vector Z_t^N, we can denote $Z_{t,d}^N = [Z_{t,2d-1}^N, Z_{t,2d}^N]$ as the two elements of the vector Z_t^N that will get multiplied by $a\mathcal{R}(\omega_d)$.

Thus, we can simplify the terms in Eq. (14).

$$
\begin{aligned}
&tr\left((S - RA^T - AR^T + AQA^T)\right) \\
&= \sum_{d=1}^{D} tr\left((S_d - (RA^T)_d - (AR^T)_d + (AQA^T)_d)\right) \\
&= \sum_{d=1}^{D}\Big[tr(S_d) - tr((RA^T)_d) \\
&\quad - tr((AR^T)_d) + tr((AQA^T)_d)\Big] \\
&= \sum_{d=1}^{D}\Big[tr(S_d) - tr(R_da\mathcal{R}(\omega_d)^T) \\
&\quad - tr(a\mathcal{R}(\omega_d)R_d^T) + tr(a\mathcal{R}(\omega_d)Q_da\mathcal{R}(\omega_d)^T)\Big] \\
&= \sum_{d=1}^{D}\Big[tr(S_d) - 2atr(R_d\mathcal{R}(\omega_d)^T) \\
&\quad + a^2tr(Q_d\mathcal{R}(\omega_d)^T\mathcal{R}(\omega_d))\Big] \qquad (15)
\end{aligned}
$$

We get the last equation because for any matrix V, $tr(V) = tr(V^T)$ and for matrices V_1, V_2, $tr(V_1V_2) = tr(V_2V_1)$. Further simplifying the terms involving $\mathcal{R}(\omega_d)$ as follows:

$$
\begin{aligned}
&tr(R_d\mathcal{R}(\omega_d)^T) \\
&= tr\left(\begin{bmatrix} R_{2d-1,2d-1} & R_{2d-1,2d} \\ R_{2d,2d-1} & R_{2d,2d} \end{bmatrix}\begin{bmatrix} \cos(\omega_d) & \sin(\omega_d) \\ -\sin(\omega_d) & \cos(\omega_d) \end{bmatrix}\right) \\
&= R_{2d-1,2d-1}\cos(\omega_d) - R_{2d-1,2d}\sin(\omega_d) \\
&\quad + R_{2d,2d-1}\sin(\omega_d) + R_{2d,2d}\cos(\omega_d) \\
&= (R_{2d-1,2d-1} + R_{2d,2d})\cos(\omega_d) \\
&\quad + (R_{2d,2d-1} - R_{2d-1,2d})\sin(\omega_d) \\
&= tr(R_d)\cos(\omega_d) + rt(R_d)\sin(\omega_d),
\end{aligned}
$$

where we define the function $rt(.)$ of a 2×2 matrix V as: $rt(V) = V_{21} - V_{12}$ and $tr(V) = V_{11} + V_{22}$. Also, $\mathcal{R}(\omega_d)^T\mathcal{R}(\omega_d) = I$. Using this, Eq. (15) gives:

$$
\begin{aligned}
&tr\left((S - RA^T - AR^T + AQA^T)\right) \\
&= \sum_{d=1}^{D} tr(S_d) - 2atr(R_d\mathcal{R}(\omega_d)^T)
\end{aligned}
$$

$$
\begin{aligned}
&\quad + a^2 tr(Q_d \mathcal{R}(\omega_d)^T \mathcal{R}(\omega_d)) \\
&= \sum_{d=1}^{D} tr(S_d) - 2a[tr(R_d)\cos(\omega_d) + rt(R_d)\sin(\omega_d)] \\
&\quad + a^2 tr(Q_d) \\
&= \sum_{d=1}^{D} tr(S_d + a^2 Q_d) \\
&\quad - 2a[tr(R_d)\cos(\omega_d) + rt(R_d)\sin(\omega_d)] \qquad (16)
\end{aligned}
$$

We can simplify the cross term between B and A in Eq. (14). Note that this term is a scalar. Therefore:

$$
\begin{aligned}
&\sum_{t=1}^{N} U_{t-1}^T B^T (Z_t^N - A Z_{t-1}^N) \\
&= \sum_{t=1}^{N} tr(U_{t-1}^T B^T (Z_t^N - A Z_{t-1}^N)) \\
&= \sum_{t=1}^{N} tr(U_{t-1}^T B^T Z_t^N) - \sum_{t=1}^{N} tr(U_{t-1}^T B^T A Z_{t-1}^N)) \\
&= \sum_{t=1}^{N} tr(U_{t-1}^T B^T Z_t^N) - \sum_{t=1}^{N} tr(A Z_{t-1}^N (B U_{t-1})^T) \\
&= \sum_{t=1}^{N} tr(U_{t-1}^T B^T Z_t^N) - tr\left(A \sum_{t=1}^{N} Z_{t-1}^N (B U_{t-1})^T\right) \\
&= \left[\sum_{t=1}^{N} tr(U_{t-1}^T B^T Z_t^N)\right] - tr(A\Phi) \\
&= \left[\sum_{t=1}^{N} tr(U_{t-1}^T B^T Z_t^N)\right] - \sum_{d=1}^{D} a tr(\mathcal{R}(\omega_d)\Phi_d) \\
&= \left[\sum_{t=1}^{N} tr(U_{t-1}^T B^T Z_t^N)\right] \\
&\quad - \sum_{d=1}^{D} a\left[tr(\Phi_d)\cos(\omega_d) - rt(\Phi_d)\sin(\omega_d)\right] \qquad (17)
\end{aligned}
$$

where, $\Phi = \sum_{t=1}^{N} Z_{t-1}^N (B U_{t-1})^T$ is a $2D \times 2D$ matrix and the trace in the final term (Eq. 17) is obtained from the following simplification:

$$
\begin{aligned}
&tr(\mathcal{R}(\omega_d)\Phi_d) \\
&= tr\left(\begin{bmatrix} \cos(\omega_d) & -\sin(\omega_d) \\ \sin(\omega_d) & \cos(\omega_d) \end{bmatrix} \begin{bmatrix} \Phi_{2d-1,2d-1} & \Phi_{2d-1,2d} \\ \Phi_{2d,2d-1} & \Phi_{2d,2d} \end{bmatrix}\right) \\
&= \Phi_{2d-1,2d-1}\cos(\omega_d) - \Phi_{2d,2d-1}\sin(\omega_d) \\
&\quad + \Phi_{2d-1,2d}\sin(\omega_d) + \Phi_{2d,2d}\cos(\omega_d) \\
&= (\Phi_{2d-1,2d-1} + \Phi_{2d,2d})\cos(\omega_d) \\
&\quad - (\Phi_{2d,2d-1} - \Phi_{2d-1,2d})\sin(\omega_d) \\
&= tr(\Phi_d)\cos(\omega_d) - rt(\Phi_d)\sin(\omega_d)
\end{aligned}
$$

Substituting Eqs. (16) and (17) in Eq (14), we get:

$$
\begin{aligned}
&G(A, B, \Sigma_w) \\
&= 2ND\log\sigma_w^2 + \frac{1}{\sigma_w^2} tr\left((S - RA^T - AR^T + AQA^T)\right) \\
&\quad - \frac{2}{\sigma_w^2}\sum_{t=1}^{N} U_{t-1}^T B^T (Z_t^N - A Z_{t-1}^N) \\
&\quad + \frac{1}{\sigma_w^2}\sum_{t=1}^{N} U_{t-1}^T B^T B U_{t-1} \\
&= 2ND\log\sigma_w^2 + \frac{1}{\sigma_w^2}\left\{\sum_{d=1}^{D} tr(S_d + a^2 Q_d)\right. \\
&\quad \left. - 2a[tr(R_d)\cos(\omega_d) + rt(R_d)\sin(\omega_d)]\right\} \\
&\quad - \frac{2}{\sigma_w^2}\left\{\sum_{t=1}^{N} tr(U_{t-1}^T B^T Z_t^N)\right. \\
&\quad \left. - \sum_{d=1}^{D} a[tr(\Phi_d)\cos(\omega_d) - rt(\Phi_d)\sin(\omega_d)]\right\} \\
&\quad + \frac{1}{\sigma_w^2}\sum_{t=1}^{N} U_{t-1}^T B^T B U_{t-1} \qquad (18)
\end{aligned}
$$

A.2. M-step

In the M-step, we maximized $G(\Theta)$ to obtain the updated value of the parameters Θ. Note that based on Eq. (10), each parameter depends on only one of the three terms. For e.g.,

$$
\begin{aligned}
&\frac{\partial G(\Theta)}{\partial C} \\
&= -\frac{1}{2}\left\{\frac{\partial G(\mu_0, \Sigma_0)}{\partial C} + \frac{\partial G(C, \Sigma_v)}{\partial C} + \frac{\partial G(A, B, \Sigma_w)}{\partial C}\right\} \\
&= -\frac{1}{2}\frac{\partial G(C, \Sigma_v)}{\partial C}
\end{aligned}
$$

Therefore, we optimized the parameters by simply considering the term in $G(\Theta)$ in which that parameter appeared.

A.2.1. Updates for μ_0, σ_0^2

From Eq. (11),

$$\frac{\partial G(\mu_0, \Sigma_0)}{\partial \mu_0}$$

$$
\begin{aligned}
&= \frac{\partial(2D\log\sigma_0^2)}{\partial\mu_0} + \frac{1}{\sigma_0^2}\frac{\partial(tr((Z_0^N-\mu_0)(Z_0^N-\mu_0)^T))}{\partial\mu_0} \\
&\quad + \frac{1}{\sigma_0^2}\frac{\partial tr(P_0^N)}{\partial\mu_0} \\
&= \frac{1}{\sigma_0^2}\frac{\partial(tr((Z_0^N-\mu_0)(Z_0^N-\mu_0)^T))}{\partial\mu_0} \\
&= \frac{1}{\sigma_0^2}(-2Z_0^N + 2\mu_0) = 0 \\
&\therefore \mu_0 = Z_0^N
\end{aligned} \tag{19}
$$

$$
\begin{aligned}
&\frac{\partial G(\mu_0,\Sigma_0)}{\partial\sigma_0^2} \\
&= \frac{\partial(2D\log\sigma_0^2)}{\partial\sigma_0^2} \\
&\quad + \frac{\partial}{\partial\sigma_0^2}\left(\frac{1}{\sigma_0^2}\right) tr((Z_0^N-\mu_0)(Z_0^N-\mu_0)^T + P_0^N) \\
&= 2D\frac{1}{\sigma_0^2} - \frac{1}{(\sigma_0^2)^2} tr((Z_0^N-\mu_0)(Z_0^N-\mu_0)^T + P_0^N) \\
&= 0 \\
&\therefore \sigma_0^2 = \frac{1}{2D} tr\Big((Z_0^N-\mu_0)(Z_0^N-\mu_0)^T + P_0^N\Big)
\end{aligned} \tag{20}
$$

A.2.2. Updates for C, σ_v^2

From Eq. (12),

$$
\begin{aligned}
&\frac{\partial G(C,\Sigma_v)}{\partial C} \\
&= (N+1)M\frac{\partial\log\sigma_v^2}{\partial C} \\
&\quad + \frac{1}{\sigma_v^2}\left[\sum_{t=0}^{N}\frac{\partial tr((X_t - CZ_t^N)(X_t-CZ_t^N)^T)}{\partial C}\right. \\
&\quad \left. + \frac{\partial tr(CP_t^NC^T)}{\partial C}\right] \\
&= \left[\sum_{t=0}^{N}\frac{\partial tr(X_tX_t^T)}{\partial C} - 2\frac{\partial tr(X_t(CZ_t^N)^T)}{\partial C}\right. \\
&\quad \left. + \frac{\partial tr\big(C(Z_t^N(Z_t^N)^T + P_t^N)C^T\big)}{\partial C}\right] \\
&= \sum_{t=0}^{N} -2X_t(Z_t^N)^T + 2C(Z_t^N(Z_t^N)^T + P_t^N) = 0 \\
&\therefore \sum_{t=0}^{N} C(Z_t^N(Z_t^N)^T + P_t^N) = \sum_{t=0}^{N} X_t(Z_t^N)^T \\
&\therefore C = \left(\sum_{t=0}^{N} X_t(Z_t^N)^T\right)\left(\sum_{t=0}^{N}(Z_t^N(Z_t^N)^T + P_t^N)\right)^{-1}
\end{aligned} \tag{21}
$$

$$
\begin{aligned}
\frac{\partial G(C,\Sigma_v)}{\partial\sigma_v^2} &= (N+1)M\frac{1}{\sigma_v^2} \\
&\quad - \frac{1}{(\sigma_v^2)^2}\sum_{t=0}^{N} tr\Big((X_t - CZ_t^N)(X_t-CZ_t^N)^T \\
&\quad + CP_t^NC^T\Big) \\
&= 0 \\
\therefore (N+1)M\frac{1}{\sigma_v^2} &= \frac{1}{(\sigma_v^2)^2}\sum_{t=0}^{N} tr\Big((X_t - CZ_t^N) \\
&\quad \times (X_t-CZ_t^N)^T + CP_t^NC^T\Big) \\
\therefore \sigma_v^2 &= \frac{1}{(N+1)M}\sum_{t=0}^{N} tr\Big((X_t - CZ_t^N)(X_t-CZ_t^N)^T \\
&\quad + CP_t^NC^T\Big)
\end{aligned} \tag{22}
$$

A.2.3. Updates for A, B

We computed the update for $\omega_d, \forall d = 1, ..., D$. From Eq (18),

$$
\begin{aligned}
&\frac{\partial G(A,B,\Sigma_w)}{\partial\omega_{d'}} \\
&= 2ND\frac{\partial\log\sigma_w^2}{\partial\omega_{d'}} + \frac{1}{\sigma_w^2}\sum_{d=1}^{D}\frac{\partial tr(S_d + a^2Q_d)}{\partial\omega_{d'}} \\
&\quad - 2a\frac{\partial}{\partial\omega_{d'}}[tr(R_d)\cos(\omega_d) + rt(R_d)\sin(\omega_d)] \\
&\quad - \frac{2}{\sigma_w^2}\left\{\sum_{t=1}^{N}\frac{\partial tr(U_{t-1}^TB^TZ_t^N)}{\partial\omega_{d'}}\right. \\
&\quad \left. - \sum_{d=1}^{D} a\frac{\partial}{\partial\omega_{d'}}[tr(\Phi_d)\cos(\omega_d) - rt(\Phi_d)\sin(\omega_d)]\right\} \\
&\quad + \frac{1}{\sigma_w^2}\sum_{t=1}^{N}\frac{\partial(U_{t-1}^TB^TBU_{t-1})}{\partial\omega_{d'}} \\
&= \frac{1}{\sigma_w^2}\sum_{d=1}^{D}(-2a)\frac{\partial}{\partial\omega_{d'}}[tr(R_d)\cos(\omega_d) + rt(R_d)\sin(\omega_d)]
\end{aligned}
$$

$$
\begin{aligned}
&+\frac{2}{\sigma_w^2}\left\{\sum_{d=1}^{D} a\frac{\partial}{\partial\omega_{d'}}[tr(\Phi_d)\cos(\omega_d)-rt(\Phi_d)\sin(\omega_d)]\right\}\\
&=\frac{-2a}{\sigma_w^2}[-tr(R_{d'})\sin(\omega_{d'})+rt(R_{d'})\cos(\omega_{d'})]\\
&\quad+\frac{2a}{\sigma_w^2}[-tr(\Phi_{d'})\sin(\omega_{d'})-rt(\Phi_{d'})\cos(\omega_{d'})]\\
&=\frac{2a}{\sigma_w^2}[tr(R_{d'}-\Phi_{d'})\sin(\omega_{d'})-rt(R_{d'}+\Phi_{d'})\cos(\omega_{d'})]\\
&=0\\
&\therefore tr(R_{d'}-\Phi_{d'})\sin(\omega_{d'})=rt(R_{d'}+\Phi_{d'})\cos(\omega_{d'})\\
&\therefore \omega_{d'}=\tan^{-1}\left(\frac{rt(R_{d'}+\Phi_{d'})}{tr(R_{d'}-\Phi_{d'})}\right)\quad\forall\, d'\in\{1,...,D\}
\end{aligned}
\tag{23}
$$

From Eq. (14),

$$
\begin{aligned}
&\frac{\partial G(A,B,\Sigma_w)}{\partial B}\\
&=2ND\frac{\partial\log\sigma_w^2}{\partial B}\\
&\quad+\frac{1}{\sigma_w^2}\frac{\partial}{\partial B}\left(tr\left((S-RA^T-AR^T+AQA^T)\right)\right)\\
&\quad-\frac{2}{\sigma_w^2}\sum_{t=1}^{N}\frac{\partial\left(U_{t-1}^T B^T(Z_t^N-AZ_{t-1}^N)\right)}{\partial B}\\
&\quad+\frac{1}{\sigma_w^2}\sum_{t=1}^{N}\frac{\partial\left(U_{t-1}^T B^T BU_{t-1}\right)}{\partial B}\\
&=-\frac{2}{\sigma_w^2}\sum_{t=1}^{N}(Z_t^N-AZ_{t-1}^N)U_{t-1}^T+\frac{1}{\sigma_w^2}\sum_{t=1}^{N}2BU_{t-1}U_{t-1}^T\\
&=0\\
&\therefore\frac{2}{\sigma_w^2}\sum_{t=1}^{N}(Z_t^N-AZ_{t-1}^N)U_{t-1}^T=\frac{2}{\sigma_w^2}B\sum_{t=1}^{N}U_{t-1}U_{t-1}^T\\
&\therefore B=\left(\sum_{t=1}^{N}(Z_t^N-AZ_{t-1}^N)U_{t-1}^T\right)\left(\sum_{t=1}^{N}U_{t-1}U_{t-1}^T\right)^{-1}
\end{aligned}
\tag{24}
$$

A.3. Identifiability

Below we describe the identifiability issue of how ω_d and $-\omega_d$ can both satify the Eq (5) by appropriately adjusting the sign of the columns of Ψ. In the proposed EM algorithm, we addressed this identifiability issue by noting that $\omega_d\in[0,\pi]$.

For simplicity, let us assume that $D=1$ and $B=0$, $w_t=0$. For a cycle corresponding to ω_d, the state transition equation is:

$$
\begin{aligned}
&\begin{bmatrix}Z_{t+1,1}\\ Z_{t+1,2}\end{bmatrix}=\begin{bmatrix}\cos(\omega_d) & -\sin(\omega_d)\\ \sin(\omega_d) & \cos(\omega_d)\end{bmatrix}\begin{bmatrix}Z_{t,1}\\ Z_{t,2}\end{bmatrix}\\
&\therefore\begin{bmatrix}Z_{t+1,1}\\ Z_{t+1,2}\end{bmatrix}=\begin{bmatrix}Z_{t,1}\cos(\omega_d)-Z_{t,2}\sin(\omega_d)\\ Z_{t,1}\sin(\omega_d)+Z_{t,2}\cos(\omega_d)\end{bmatrix}
\end{aligned}
\tag{25}
$$

For a cycle corresponding to $-\omega_d$ and latent state denoted by $\bar{Z}_t$, the state transition equation is:

$$
\begin{aligned}
&\begin{bmatrix}\bar{Z}_{t+1,1}\\ \bar{Z}_{t+1,2}\end{bmatrix}=\begin{bmatrix}\cos(-\omega_d) & -\sin(-\omega_d)\\ \sin(-\omega_d) & \cos(-\omega_d)\end{bmatrix}\begin{bmatrix}\bar{Z}_{t,1}\\ \bar{Z}_{t,2}\end{bmatrix}\\
&\therefore\begin{bmatrix}\bar{Z}_{t+1,1}\\ \bar{Z}_{t+1,2}\end{bmatrix}=\begin{bmatrix}\cos(\omega_d) & \sin(\omega_d)\\ -\sin(\omega_d) & \cos(\omega_d)\end{bmatrix}\begin{bmatrix}\bar{Z}_{t,1}\\ \bar{Z}_{t,2}\end{bmatrix}\\
&\therefore\begin{bmatrix}\bar{Z}_{t+1,1}\\ \bar{Z}_{t+1,2}\end{bmatrix}=\begin{bmatrix}\bar{Z}_{t,1}\cos(\omega_d)+\bar{Z}_{t,2}\sin(\omega_d)\\ -\bar{Z}_{t,1}\sin(\omega_d)+\bar{Z}_{t,2}\cos(\omega_d)\end{bmatrix}
\end{aligned}
\tag{26}
$$

In the RHS of Eq (26), replace $\bar{Z}_{t,1}=Z_{t,1}$ and $\bar{Z}_{t,2}=-Z_{t,2}$.

$$
\begin{aligned}
&\begin{bmatrix}\bar{Z}_{t,1}\cos(\omega_d)+\bar{Z}_{t,2}\sin(\omega_d)\\ -\bar{Z}_{t,1}\sin(\omega_d)+\bar{Z}_{t,2}\cos(\omega_d)\end{bmatrix}\\
&=\begin{bmatrix}Z_{t,1}\cos(\omega_d)-Z_{t,2}\sin(\omega_d)\\ -Z_{t,1}\sin(\omega_d)-Z_{t,2}\cos(\omega_d)\end{bmatrix}\\
&=\begin{bmatrix}Z_{t,1}\cos(\omega_d)-Z_{t,2}\sin(\omega_d)\\ -(Z_{t,1}\sin(\omega_d)+Z_{t,2}\cos(\omega_d))\end{bmatrix}\\
&=\begin{bmatrix}Z_{t+1,1}\\ -Z_{t+1,2}\end{bmatrix}\quad\text{(From Eq (25))}
\end{aligned}
$$

Thus, the pairs ω_d and $[Z_{t,1},Z_{t,2}]$, as well as $-\omega_d$ and $[Z_{t,1},-Z_{t,2}]$ both satisfy the state transition Eq (4), which gives rise to the identifiability issue mentioned at the beginning of this subsection.

A.4. Update for general A (vanilla EM)

In the general setting in which A is not assumed to have the block diagonal structure with $\mathcal{R}(\omega_d)$ as blocks, the update for A is giving by the following calculation.

$$
\begin{aligned}
\frac{\partial G(A,B,\Sigma_w)}{\partial A}&=2ND\frac{\partial\log\sigma_w^2}{\partial A}\\
&+\frac{1}{\sigma_w^2}\frac{\partial tr\left((S-RA^T-AR^T+AQA^T)\right)}{\partial A}\\
&-\frac{2}{\sigma_w^2}\sum_{t=1}^{N}\frac{\partial U_{t-1}^T B^T(Z_t^N-AZ_{t-1}^N)}{\partial A}\\
&+\frac{1}{\sigma_w^2}\sum_{t=1}^{N}\frac{\partial U_{t-1}^T B^T BU_{t-1}}{\partial A}
\end{aligned}
$$

$$= \frac{1}{\sigma_w^2}\frac{\partial tr\left((S - RA^T - AR^T + AQA^T)\right)}{\partial A} - \frac{2}{\sigma_w^2}\sum_{t=1}^{N}\frac{\partial U_{t-1}^T B^T (Z_t^N - AZ_{t-1}^N)}{\partial A}$$

$$= \frac{1}{\sigma_w^2}(-R - R + 2AQ) + \frac{2}{\sigma_w^2}\sum_{t=1}^{N} BU_{t-1}(Z_{t-1}^N)^T$$

$$\therefore \frac{2}{\sigma_w^2}\sum_{t=1}^{N} BU_{t-1}(Z_{t-1}^N)^T = \frac{1}{\sigma_w^2}(2R - 2AQ)$$

$$\therefore A = \left(R - \sum_{t=1}^{N} BU_{t-1}(Z_{t-1}^N)^T\right) Q^{-1} \quad (27)$$

Appendix B. Synthetic data

B.1. Data generation

We generated synthetic data to assess whether the proposed EM algorithm could recover ground truth (known) parameters. We used the forward model from Eq (4)to generate synthetic data. The parameters were chosen based on preliminary analysis such that: (i) the synthetic data included multiple cycles in $\mathbf{Z}$ and $\mathbf{X}$ and (ii) $\mathbf{U}$ demonstrated a significant effect on progression. A seizure was generated at time t with a small probability p_{sz} if the overall seizure risk ($\sum_{j=1}^{2D} Z_{t,j}$) was greater than a threshold (τ). p_{sz} and τ were chosen to obtain a sufficient number of seizures to enable a reasonable estimation of B. Whenever this resulted in the generation of a seizure in the model, the characteristics of the seizure ($U_t \in \mathbb{R}^M$) were drawn from a multivariate Gaussian distribution. $U_t = \mathbf{0}$ if there was no seizure. The data was of length N.

B.2. Parameter estimation using EM

The proposed EM and vanilla EM both estimated cycle periods accurately (cycle period (days): ground truth - (10, 25, 45), proposed - (10, 24.96, 45.02), vanilla - (10.05, 25.27, 44.5)). However, the estimated A for vanilla EM was different from the ground truth (Figure 3), and the estimated A for proposed EM was similar to the ground truth. This was a consequence of the identifiability issue with vanilla EM. The structure of A in vanilla EM resulted in cycles of different periods being represented together with uneven weights in Z_t. As a result, the overall seizure risk obtained by $\sum_j Z_{t,j}$ did not accurately reflect the true risk. Even though vanilla EM recovered the cycle periods accurately, it was unable to track seizures (Figure 5). The proposed EM performed better than vanilla EM in tracking seizures, as seen visually as well as reflected numerically by the larger Z-distance (Figure 5).

B.3. Stability analysis

To further understand the performance of the proposed EM algorithm, we varied the data characteristics and estimated model parameters. Synthetic data was generated that varied one of (i) data length (N), (ii) missingness, (iii) σ_w^2, and (iv) norm of eigenvalues of A (a). To assess the effect on the EM performance, we evaluated the MSE of the estimated B and C (Figure 4). As the data length N increased, estimation error for C increased. That could be because for large N, $||Z_t||^2$ becomes large, which could lead to numerical difficulties in estimating C. As expected, MSE of B and C increased as missing data increased, highlighting the challenge of estimation when a large percentage of data is missing.

Appendix C. NeuroVista data

C.1. Intracranial EEG Data

Six out of 15 participants in the NeuroVista study were excluded from this analysis due to significant data drops, which could affect the analysis of seizure clusters. The remaining nine patients had an average recording duration of 550 $\pm$ 208 days (Table 2).

To manage the amount of data used for feature computation, we extracted one hour of data from each day (24 hours). To reduce the effect of circadian cycles on the analysis, the same hour of data was extracted from all the days for a participant. This patient-specific hour was identified based on domain knowledge. We consulted a domain expert (V.K.) to select the hour when seizures were less likely to occur.

C.2. iEEG pre-processing

Each hour of data was divided into 10-second segments, resulting in 360 segments for each hour. The following pre-processing steps were applied to each segment: (i) referencing, (ii) missing data imputation, (iii) filtering, and (iv) normalization.

1. We referenced the signal using a bipolar montage by taking the difference of the raw signal from adjacent contacts on a strip. This resulted in 12

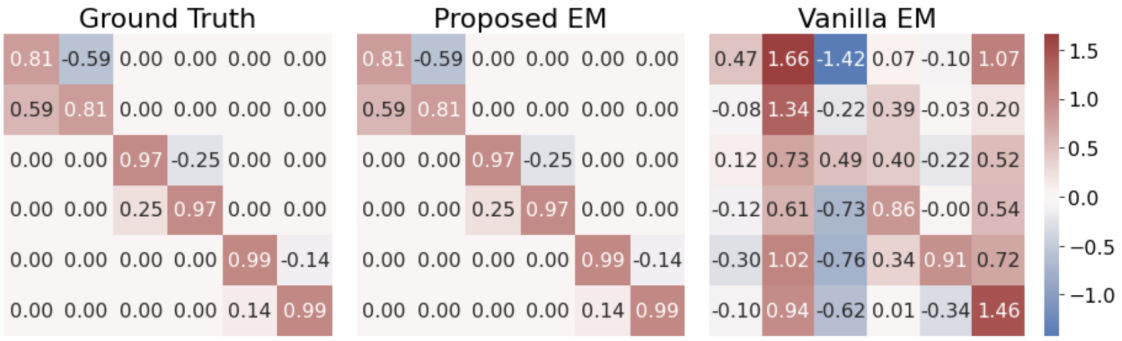

Figure 3: Synthetic data: A matrix for (left) ground truth, (middle) proposed EM, (right) vanilla EM.

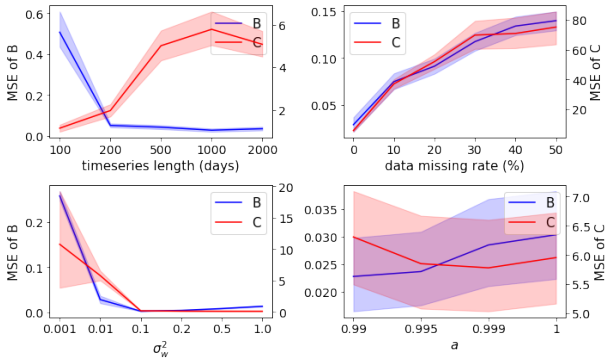

Figure 4: Synthetic data: MSE of B and C for different data characteristics.

bipolar pairs (Saboo et al., 2023). We refer to each bipolar pair as an "electrode".

2. Missing data within a segment was handled in two ways. If the fraction of missing data within a segment was < 0.5, the missing values were imputed using the median of the signal in that hour. Otherwise, the entire segment was ignored from the analysis. Imputation was performed before filtering and normalization. Imputation within a segment was performed to enable filtering of the signal into different frequency bands.

3. The signal from each electrode was filtered into non-overlapping frequency bands using forward-backward second-order Butterworth filters: delta (0.5 - 4Hz) (δ), theta (4 - 8Hz) (θ), alpha (8 - 12Hz) (α), sigma (12 - 16Hz) (σ), beta (16 - 25Hz) (β), low gamma (30 - 60Hz) (γ_l), high gamma (60 - 80Hz) (γ_h).

4. The signals were normalized to have zero mean and unit variance to compare them across electrodes and over days. Normalization was done separately for each segment and electrode.

The order of normalization and filtering was different for the univariate and bivariate features. For the power-in-band univariate feature, the signal was first normalized and then filtered. This allowed extracting power in a band relative to other bands. For bivariate features, the signal was filtered first and then normalized separately for each band. This enabled minimizing the impact of discrete approximations made for REN computation. The order of filtering and normalization does not affect PLV or correlation coefficient.

C.3. Feature extraction

Univariate and bivariate features were extracted from each 10-second segment. Values within a segment imputed during pre-processing were ignored during feature computation to minimize the effect of imputation on feature values. We extracted the following features: (i) power in band (PIB), which is the squared amplitude of the signal; (ii) relative entropy (REN), which is the distance between the amplitude distributions between pairs of electrodes (Saboo et al., 2022); (iii) phase locking value (PLV), which is the average instantaneous phase difference between signals from a pair of electrodes (Khambhati et al., 2021); and (iv) Pearson correlation coefficient (PCC), i.e., the correlation between signals at two electrodes.

C.4. Feature aggregation

We obtained features from each of the 360 segments within an hour. To obtain an aggregate value for each feature in an hour, we found the median value

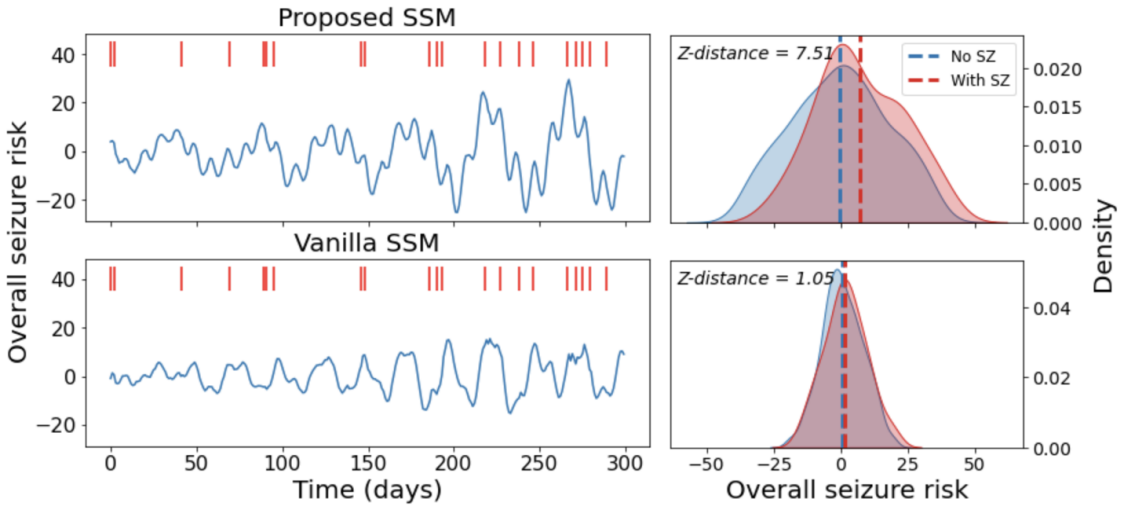

Figure 5: Synthetic data: (Left) Overall seizure risk inferred by the model (blue) and seizures (red). (Right) Distribution of overall seizure risk when seizures occurred (red) and when seizures did not occur (blue). Mean of the two distributions used for computed Z-distance is shown. Top panels shows proposed SSM, bottom panels show vanilla SSM.

of the feature across the 360 segments. We used the median value because it is more robust to outliers than the average. Segments with more than 50% of missing time points were ignored while computing the median. We ignored segments that overlapped with seizures or were within 5 minutes before seizure onset or within 1 hour after seizure termination. Aggregation was performed separately for each feature, band, and electrode (pair). Thus, each hour of data was represented by 1470 features (12 (electrodes) $\times$7 (bands) univariate features + 66 (electrode pairs) $\times$7 (bands) $\times$3 (feature types) bivariate features).

C.5. Feature selection

To obtain X_t, we selected a few features that demonstrated cycles for the ease of model fitting based on the cycle period of seizures clusters. Feature selection was done separately for each patient. (i) We obtained the three most prominent multiday cycle periods of clustered seizures. We selected iEEG features that had multiday cycles of the same periodicity as seizure cluster cycles. This resulted in several features being selected for each cycle period. (ii) We further reduced the number of features for each cycle period to balance the representation of each cycle in the model. For each cycle period, the three iEEG features with the smallest p-value for the given period from the wavelet analysis were obtained. This resulted in upto nine iEEG features that were represented by X_t in the model.

Table 2: Patient information. Columns: Patient number, duration of iEEG data, % of samples missing, number of seizures, number of clustered seizures.

PID	Data Length (days)	Missing Rate(%)	# Sz	# Clus.
1	768	27.84	169	136
2	730	18.36	45	8
3	185	38.70	660	650
4	559	40.43	727	714
5	395	24.56	280	215
6	374	11.23	860	841
7	729	3.28	33	9
8	747	22.19	762	661
9	465	3.65	101	26

C.6. Seizure detection

Seizures were detected from the iEEG recordings using a published methodology (Sladky et al., 2022). Seizures detected within a minute of each other were

combined into a single seizure. This procedure resulted in an average of 404.2 ± 322.4 seizures per participant. The average duration of the seizures was 40.7 ± 79.7s. Features representing seizures were extracted as described in below and aggregated across seizures within a day to obtain U_t.

C.7. Feature extraction for seizures

The pre-processing steps in Appendix C.2 were applied to seizure iEEG, although segmenting was modified slightly. Since seizures can be of arbitrary duration, seizures were divided into 10-second segments from the seizure onset. For the last few seconds of a seizure that could not fully occupy a 10-second segment, if the length was less than 3 seconds, it was included as part of the previous segment. It was considered a new segment if it was more than 3 seconds. Feature extraction and aggregation were performed as described in Appendix C.3.

There can be no or multiple seizures for each day, and the seizures can be outside the 1-hour window we picked for feature extraction. Therefore, we prepared the seizure features U_t with the following steps: (i) We considered seizures that happened anytime during the day, no matter whether they fell in the 1-hour window from which iEEG features were computed or not. (ii) When there was no seizure during day t, the seizure feature U_t was set as a $\mathbf{0}$ vector. (iii) When there were multiple seizures during day t, we extracted the features $U_t^{(i)}$ for each seizure i and computed the seizure feature U_t for day t as the summation of each seizure $U_t = \sum_i U_t^{(i)}$ to accumulate the strength of multiple seizures.

Appendix D. Cycles in iEEG features

D.1. Approach: Wavelet analysis

We performed wavelet analysis to investigate whether there were cycles in the iEEG features. Wavelet analysis was done separately for each feature and patient (Figure 6). (i) First, the time series of the feature over days was linearly detrended to remove any mean component or linear drift over time. (ii) Secondly, we computed a continuous wavelet transform (CWT) of the detrended timeseries using a Morlet wavelet with $\omega_0 = 6$. The scale of the wavelets spanned five octaves (2-4 days, 4-8 days, ..., 32 - 64 days) with 12 sub-octaves per octave. We restricted the analysis to periods of up to 64 days to obtain at least 3 cycles of that period in each participant. (iii) Next, we computed the power at each scale by averaging the squared amplitude of the CWT over time to obtain a periodogram. (iv) We assessed the statistical significance of peaks in the periodogram assuming a red noise model (Torrence and Compo, 1998).

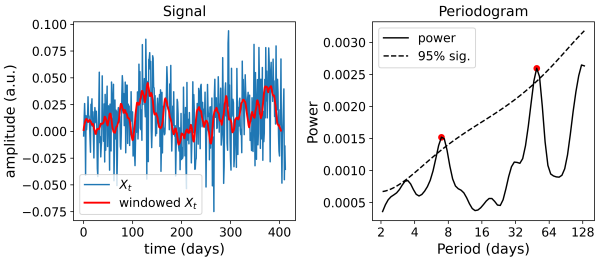

Figure 6: Wavelet analysis. (Left) An iEEG feature of Patient 9. (Right) The given feature's wavelet periodogram. Peaks in the periodogram above the significance threshold are shown in red (6.9 days and 49.5 days).

If a feature timeseries had missing data for some days, then a technique similar to krigging was used for imputation (Baud et al., 2018). For a gap of contiguous missing values, we obtained windows of data of the same length as the gap adjacent to the gap on its left and right. The value at each time point in the gap was sampled from a Gaussian distribution. The mean of the distribution changed linearly between the mean of the left and right windows. The standard deviation was the average of standard deviation of the two windows. Imputation was performed only for the wavelet analysis.

D.2. Results

Cycles of different periods were detected across iEEG features and patients (Figure 7). The number of features that contained a cycle of a given multiday period was different across patient. Cycles were observed across different feature types, electrodes, and frequency bands. This suggested that multiday cycles are present in inter-ictal (between seizure) iEEG feature timeseries.

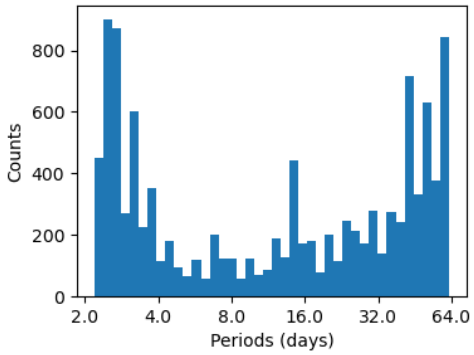

Figure 7: Histogram of cycle periods in iEEG features across all patients.

Appendix E. Cycles in seizures

E.1. Approach: R-value analysis

We investigated whether there were cycles in seizures in the dataset used for this study. Previous studies have identified circadian and multidien cycles in seizure timings (Gregg et al., 2021; Baud et al., 2018; Karoly et al., 2018). Cycles were identified using R-value computed for different periods (Gregg et al., 2021; Baud et al., 2018). R-value measures the circular non-uniformity of events. We computed the R-value for integer periods between 2 to 64 days.

Since *isolated* and *clustered* seizures have different dynamics (Saboo et al., 2022), we investigated whether they occur in cycles independently. We computed cycles for (i) isolated seizures and (ii) clustered seizures separately, and also for (iii) all the seizures combined. Seizures within 24 hours of each other, i.e., with an inter-seizure interval of < 24 hours, were considered part of a cluster (Saboo et al., 2022). The remaining seizures were classified as isolated.

We used a Rayleigh test to assess the statistical significance of the R-values. The test determines whether there is a unimodal deviation from circular uniformity by rejecting the null hypothesis that events are uniformly distributed around the circle (Gregg et al., 2021). Rayleigh test was conducted for each period and seizure type. Multiple comparisons were accounted for by using FDR correction applied to all the comparisons within a participant. Among the periods with significant r-values, we picked the ones with peak r-values among their neighbors.

E.2. Results

For Patient 9, several R-values were statistically significant for the clustered seizures and when all seizures were combined (Figure 8(a)), indicating multiday cycles. The largest r-value was observed for a 50-day cycle in clustered seizures. No cycles were detected in the isolated seizures.

Cycles in seizure clusters were observed in eight out of nine patients (Figure 8(b)). Cycles in all seizures combined were observed in six patients, and cycles in isolated seizures were observed only in two patients. Thus, seizure clusters are more likely to occur in multiday cycles than isolated seizures. Multiday cycle periods and the number of cycles in clustered seizures were patient-specific (Figure 8(c)).

For developing and validating the model, we selected the three cycle periods with the largest r-value for each patient. When a patient only had two multiday seizure cycle periods, both were chosen. Patient 2 and Patient 7 only had one multiday cycle. Therefore, we selected another cycle by picking the one with the highest r-value and at least 10 days away from the significant cycle period. Patient 5 had no significant multiday cycles, so we picked 2 cycle periods with the highest r-values that were at least 10 days apart from each other.

Appendix F. NeuroVista: Results

F.1. Baseline model

Vanilla SSM: We compared with a vanilla SSM that did not constrain the structure of A and $\Sigma_w = 0.01I$. The model was trained with vanilla EM. The dimensionality of the latent state was the same as the proposed model ($2D$). Training and hyper-parameter settings of vanilla SSM were the same as the proposed SSM except for A's initialization. For synthetic data, 100 initializations (seeds) of the model were trained for 200 epochs each. For real data, 60 initializations were trained for 300 epochs each. For each seed, the model corresponding to the minimum validation negative log likelihood was considered. We picked the seed for which recovered angels ω_d computed from the eigenvalues of A were closest to the ground truth cycle ω_ds (in the mean squared sense). In several cases (seeds as well as patients), we observed that the norm of largest eigenvalue of A was > 1, indicating that the model diverged. We excluded seeds with the norm of the largest eigenvalue > 1. There were four

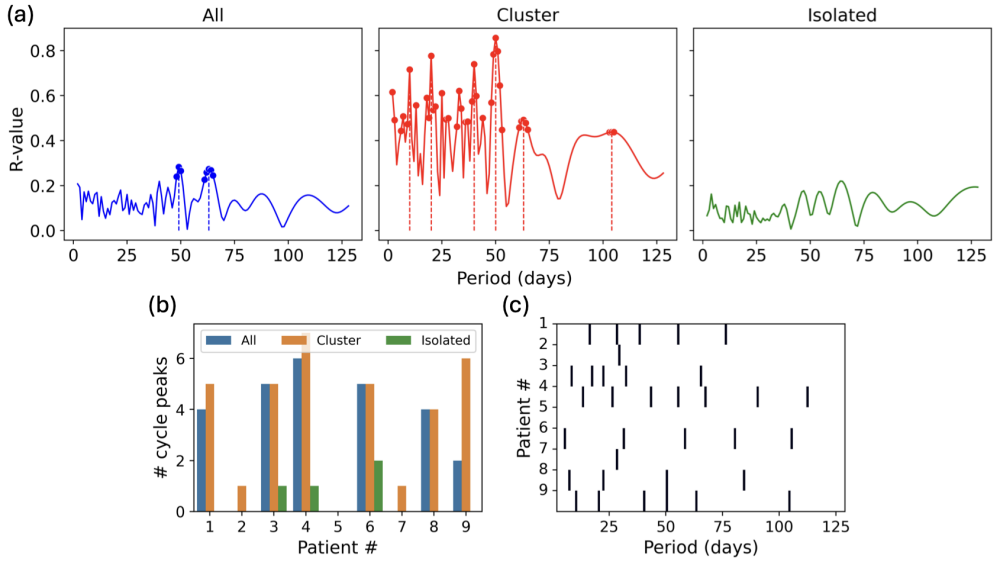

Figure 8: Cycles in seizure clusters. (a) R-value of seizures for different cycle periods for Patient 9. R-values are shown for (left) all seizures, (middle) seizure clusters, (right) isolated seizures. Significant R-values are marked. Peaks of significant R-values correspond to multiday cycles. (b) The number of multiday cycles for each patient and seizure type. (c) Multiday cycle periods for clustered seizures.

patients for whom no seed obtained a non-divergent vanilla SSM.

MK SSM: We compared with the Matsuda and Komaki (2017) model, which also constrains the structure of A. However, they assumed that at least one feature includes all the multiday cycles, with the observation matrix C defined as:

$$C = \begin{bmatrix} 1 & 0 & 1 & 0 & \dots & 1 & 0 \\ c_{21,1} & c_{21,2} & c_{22,1} & c_{22,2} & \dots & c_{c_{2D},1} & c_{2D,2} \\ \vdots & \vdots & \vdots & \vdots & \ddots & \vdots & \vdots \\ c_{J1,1} & c_{J1,2} & c_{J2,1} & c_{J2,2} & \dots & c_{c_{JD},1} & c_{JD,2} \end{bmatrix}$$

where J is the number of features, and D is the number of multiday cycles. They fixed the coefficients for the first feature to be 0s and 1s to ensure parameter identifiability. In our implementation, we set $\Sigma_w = 0.01I$. The dimensionality of the latent state matched that of the proposed model ($2D$). The training process and hyperparameter settings for MK SSM was the same as those used for the proposed SSM, except for the update of C. The update equation for C in the EM algorithm was as follows:

$$C_{1:J} = \left(\sum_{t=0}^{N} X_{t,1:J} (Z_t^N)^T \right) \left(\sum_{t=0}^{N} Z_t^N (Z_t^N)^T + P_t^N \right)^{-1}$$

We updated every row in C except for the first row using all features of X_t except for the first one.

LSTM: We compared our model with a nonlinear baseline, the long short-term memory (LSTM) model. LSTM was designed to take both iEEG features X_t and seizure features U_t as input, with $2D$ hidden states and a dense layer to predict the iEEG features for the following day, matching the structure of the proposed SSM. We implemented LSTM using the *tensorflow.keras* package, trained it with the *Adam optimizer*, and used mean squared error (MSE) as the loss function. The model was trained for 300 epochs with a batch size of 16.

F.2. Alignment between seizure clusters and inferred seizure risk

We measured the alignment between seizure clusters and inferred seizure risk. We computed a metric to compare two distributions, which we referred to as *Z-distance*. For a patient, the Z-distance is the difference in the mean of the normalized overall seizure risk ($\hat{z}_t$) when seizure clusters occurred (μ_c) and when seizure clusters did not occur (μ_{nc}). Let the set of days on which seizure clusters occurred be $\mathcal{T}_c$, the days when seizure clusters did not occur be $\mathcal{T}_{nc}$, and

$\mathcal{T} = \mathcal{T}_c \cup \mathcal{T}_{nc}$. Then,

$$\mu_z = \frac{1}{|\mathcal{T}|}\sum_{t\in\mathcal{T}}\sum_j Z_{t,j}, \quad \sigma_z^2 = \frac{1}{|\mathcal{T}|}\left(\sum_j Z_{t,j} - \mu_z\right)^2$$

$$\hat{z}_t = \frac{\sum_j Z_{t,j} - \mu_z}{\sigma_z}$$

$$\mu_c = \frac{1}{|\mathcal{T}_c|}\sum_{t\in\mathcal{T}_c}\hat{z}_t, \quad \mu_{nc} = \frac{1}{|\mathcal{T}_{nc}|}\sum_{t\in\mathcal{T}_{nc}}\hat{z}_t$$

$$Z - distance = |\mu_c - \mu_{nc}|$$

A higher Z-distance implies that the seizure clusters occur (on average) when the overall seizure risk is higher than the average overall seizure risk. This is in concordance with the hypothetical model of Figure 1(a). We used magnitude of the difference because the proposed EM identifies cycles only upto a sign. Thus, the overall seizure risk could be either the same sign as the true overall risk, or the negative of it. Importantly, seizure clusters should occur at the extremum (or close to it) of the overall seizure risk. The intuition behind the Z-distance metric can be see in Figure 5.

Table 3: Results on real data of each patient (PID): Accuracy of the proposed SSM (PM), vanilla SSM (VM), and MK SSM (MK) in recovering multiday cycles. (–) denotes patients for whom the model diverged. Better performance is shown in bold.

PID	**Multi-day cycle period (days)**	**Cycle accuracy (weighted MSE)**		
	Ground Truth	PM	VM	MK
1	(16, 28, 38)	**0.28**	–	0.31
2	(16, 29)	**0.61**	–	0.81
3	(22, 32)	**0.01**	12.6	0.52
4	(26, 43, 55)	**0.50**	27.69	0.21
5	(18, 32, 51)	**0.49**	–	0.13
6	(5, 31)	**0.09**	4.07	0.03
7	(18, 28)	**0.27**	4.92	0.78
8	(7, 22, 50)	**0.49**	–	0.20
9	(20, 40, 50)	**0.36**	19.5	0.52

F.3. RL-based treatment optimization

We implemented the RL framework using OpenAI's Gym framework (Brockman et al., 2016). Since we had access to the environment, we used TRPO, a model-free on-policy learning algorithm (Schulman et al., 2015). The RL agent was trained for 20 episodes with a batch size of 128, with each episode being 400 time points in duration. The policy network was parameterized using a multi-layer perceptron with 2 hidden layers of 16 units each. We used the default hyperparameters provided for TRPO. The stimulation mean was set to 5% of the mean amplitude of seizures U_t, and the variance was set to 400% of the variance across seizures.

We determined the seizure threshold τ as the value that best separated the distribution of overall seizure risk ($\sum_i Z_{t,i}$) of days with seizure clusters versus that of days without seizure clusters.

We investigated the outcome for Patient 9 if a stimulation with RL had been applied from day 50 onwards. Kalman filtered Z_{50}^{50} obtained from the real data was used as the initial state of the system. We observed that adaptive stimulation reduced the amplitudes of the inferred seizure risk cycles *in silico* (Figure 10(b)). Within 105 days of stimulation (day 155), the overall seizure risk was below the seizure threshold τ for most days. The corresponding reward of the model also reached close to the maximum (0) after approximately 105 days.

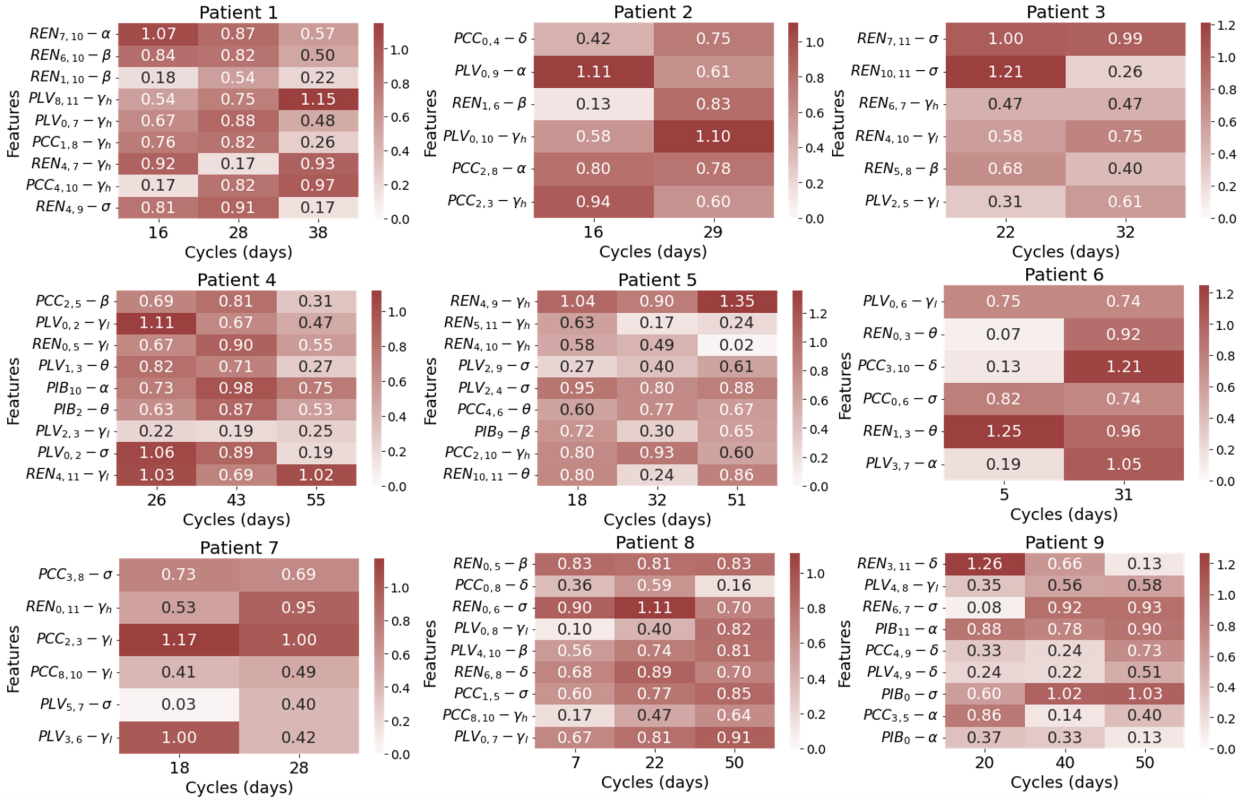

Figure 9: Coefficients of the input matrix B for all patients. Feature abbrv. format: $type_{electrode(s)} - band$.

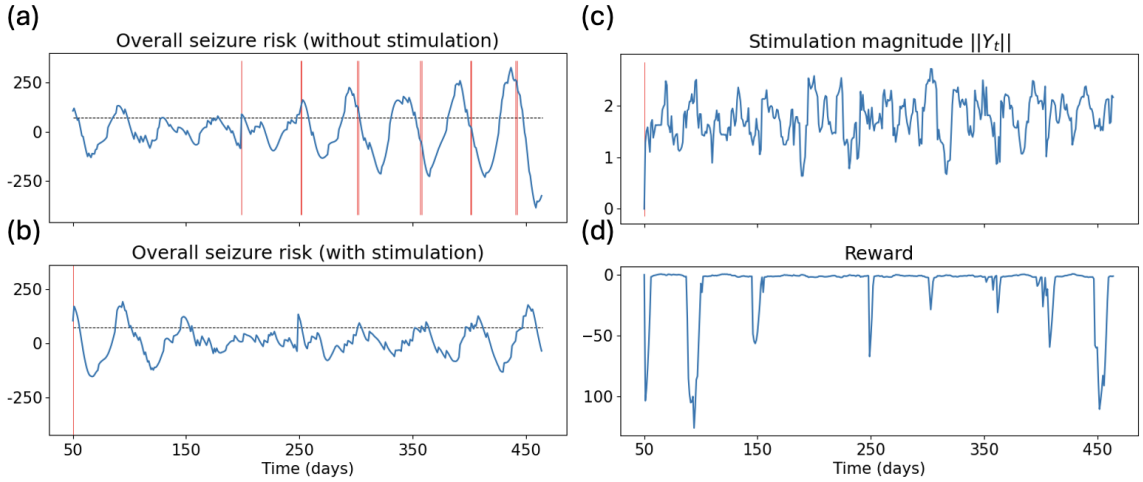

Figure 10: *In silico* adaptive brain stimulation for Patient 9. (a) Overall seizure risk inferred from Patient 9's iEEG data. Red lines show seizure clusters observed in the data. (b,c,d) show the result if the patient received stimulation treatment from the RL framework. (b) Overall seizure risk after stimulation generated by the dynamics in Eq (6). (c) The magnitude of stimulation $||Y_t||$. (d) Reward received by the RL agent over time.